iScience

CellPress
OPEN ACCESS

Article

Increased glycine contributes to synaptic dysfunction and early mortality in Nprl2 seizure model

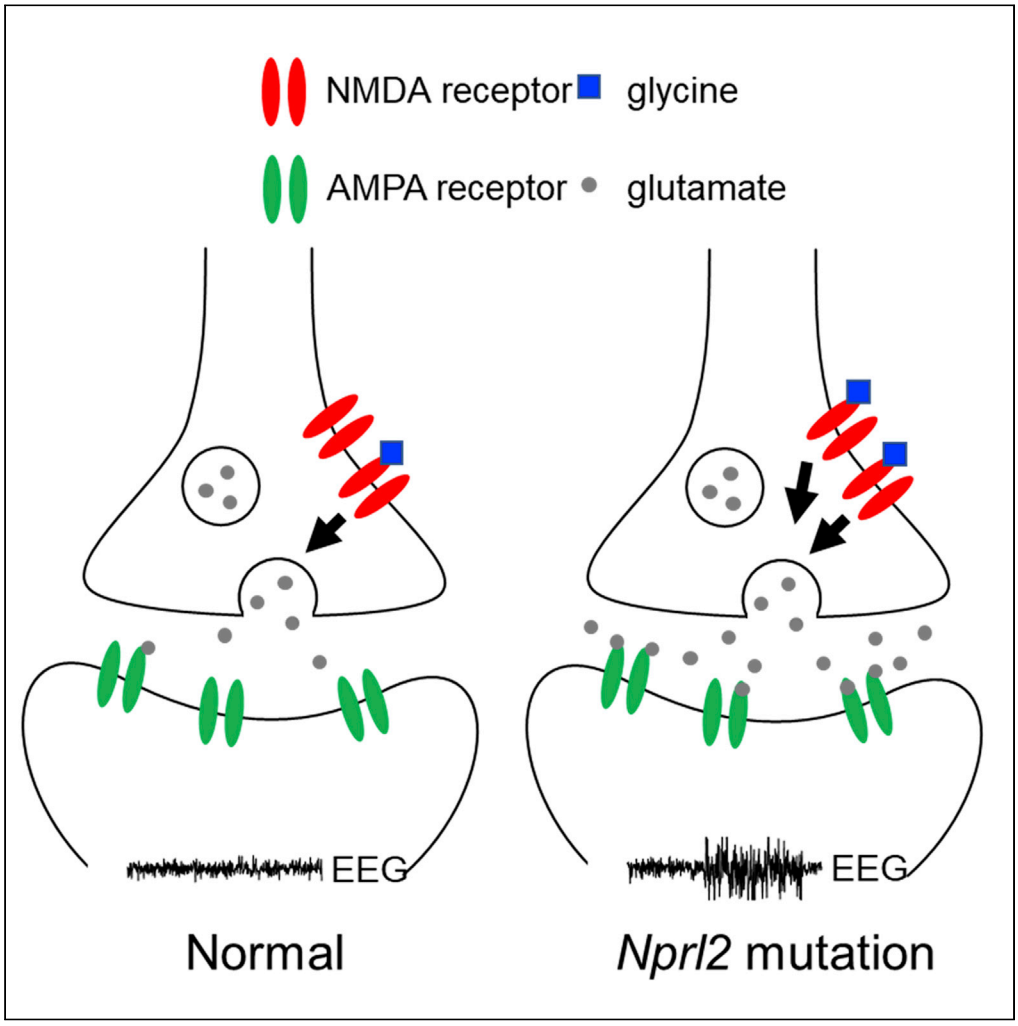

Brianne Dentel, Lidiette Angeles-Perez, Chongyu Ren, ..., Kimberly M. Huber, Benjamin P. Tu, Peter T. Tsai

peter.tsai@utsouthwestern.edu

Highlights

Neocortical loss of *Nprl2* leads to mTORC1-dependent seizures and decreased survival

Conditional *Nprl2* mutants show increased synaptic excitation and decreased inhibition

Neurotransmitter glycine is increased in *Nprl2* mutant neocortex

Glycine actions at NMDA receptor contribute to synaptic and survival phenotypes

Dentel et al., iScience *25*, 104334
May 20, 2022
https://doi.org/10.1016/j.isci.2022.104334

iScience

CellPress
OPEN ACCESS

Article

Increased glycine contributes to synaptic dysfunction and early mortality in Nprl2 seizure model

Brianne Dentel,[1,5] Lidiette Angeles-Perez,[1,5] Chongyu Ren,[1] Vikram Jakkamsetti,[1] Andrew J. Holley,[2] Daniel Caballero,[1] Emily Oh,[1] Jay Gibson,[2] Juan M. Pascual,[1] Kimberly M. Huber,[2] Benjamin P. Tu,[3] and Peter T. Tsai[1,2,4,6,*]

SUMMARY

Targeted therapies for epilepsies associated with the mTORC1 signaling negative regulator GATOR1 are lacking. NPRL2 is a subunit of the GATOR1 complex and mutations in GATOR1 subunits, including *NPRL2*, are associated with epilepsy. To delineate the mechanisms underlying NPRL2-related epilepsies, we created a mouse (*Mus musculus*) model with neocortical loss of *Nprl2*. Mutant mice have increased mTORC1 signaling and exhibit spontaneous seizures. They also display abnormal synaptic function characterized by increased evoked and spontaneous EPSC and decreased evoked and spontaneous IPSC frequencies, respectively. Proteomic and metabolomics studies of *Nprl2* mutants revealed alterations in known epilepsy-implicated proteins and metabolic pathways, including increases in the neurotransmitter, glycine. Furthermore, glycine actions on the NMDA receptor contribute to the electrophysiological and survival phenotypes of these mice. Taken together, in this neuronal *Nprl2* model, we delineate underlying molecular, metabolic, and electrophysiological mechanisms contributing to mTORC1-related epilepsy, providing potential therapeutic targets for epilepsy.

INTRODUCTION

In humans, mutations in *NPRL2* alone are linked to familial focal epilepsy (OMIM# 607072) (Ricos et al., 2016; Shen et al., 2019). NPRL2 is an essential subunit of a larger complex GATOR1, which is a negative regulator of the mTOR pathway. Several studies have found that *Nprl2* regulates amino acid and TCA cycle metabolism in yeast, *Drosophila*, mouse muscle, and mouse embryonic fibroblasts (Laxman et al., 2014; Moloney et al., 2021). Although two recent studies with conditional knockout mouse models of *Nprl2* have shown these mice develop seizures (Hui et al., 2022; Ishida et al., 2021), very little is known about how loss of *Nprl2* results in seizures and/or the metabolic and molecular contributions to these mechanisms.

The mechanistic target of rapamycin complex 1 (mTORC1) pathway, in which NPRL2 plays a major role, is broadly implicated in genetic epilepsies (Crino, 2015; Kim and Lee, 2019; Marsan and Baulac, 2018). mTORC1 is a regulator of protein synthesis and metabolism in response to growth factors, insulin, and amino acids (Düvel et al., 2010; Holz et al., 2005; Kim et al., 2011; Laxman et al., 2014; Ma et al., 2008). mTORC1 has critical roles in multiple processes within the nervous system (Lasarge and Danzer, 2014; Lipton and Sahin, 2014). Regulators of mTORC1 activity, including tuberous sclerosis complex 1/2 (TSC1/2), phosphatase and tensin homolog (PTEN), protein kinase B (AKT), and GAP activity toward rags 1 (GATOR1) among others have all been implicated in genetic epilepsies and neurodevelopmental disorders associated with epilepsy (Bar-Peled et al., 2013; Panchaud et al., 2013). While one arm of the regulation of mTORC1 is sensitive to the presence of growth factors and insulin, GATOR1 is uniquely sensitive to amino acids. GATOR1 negatively regulates mTORC1 activity through GAP activity which prevents the mTORC1 complex from translocating to the lysosome (Chen et al., 2017). Therefore, loss of function of this essential negative regulator GATOR1 yields hyperactivation of mTORC1 and mTORC1 insensitivity to amino acid availability (Chen et al., 2017; Dokudovskaya and Rout, 2015). In addition, although other mTORC1

[1]Department of Neurology, UT Southwestern Medical Center, Dallas, TX 75235, USA

[2]Department of Neuroscience, UT Southwestern Medical Center, Dallas, TX 75235, USA

[3]Department of Biochemistry, UT Southwestern Medical Center, Dallas, TX 75235, USA

[4]Departments of Pediatrics and Psychiatry, UT Southwestern Medical Center, Dallas, TX 75235, USA

[5]These authors contributed equally

[6]Lead contact

*Correspondence: peter.tsai@utsouthwestern.edu

https://doi.org/10.1016/j.isci.2022.104334

regulators are perhaps better known and studied, the GATOR1 complex is highly evolutionarily conserved through yeast, unlike the TSC1/2 complex (Dokudovskaya et al., 2011; Tatebe and Shiozaki, 2017; Wu and Tu, 2011).

Mutations in GATOR1 complex genes are linked to familial epilepsy (Baldassari et al., 2016; Weckhuysen et al., 2016) and contribute to over 12% of focal epilepsies, 54% of whom have medically resistant epilepsy (Baldassari et al., 2019; Dibbens et al., 2013). Each subunit of GATOR1—DEP domain containing 5 (DEPDC5), nitrogen permease regulator-like 2 and 3 (NPRL2 and NPRL3)—is essential to its function (Sutter et al., 2013; Wu and Tu, 2011), increased mTORC1 activity results from deleterious mutations in any of these subunits (Weckhuysen et al., 2016), and each subunit is associated with clinical epilepsy (Baldassari et al., 2019; Ricos et al., 2016). Conditional mutants of *Depdc5* and *Nprl3* in mice exhibit increased susceptibility to seizure activity, and it has been recently demonstrated that loss of *Depdc5* in early progenitors of excitatory and glial cells results in spontaneous seizures (de Calbiac et al., 2018; Klofas et al., 2020; Yuskaitis et al., 2018).

Although NPRL2 mutations are associated with epilepsy and NPRL2 is GATOR1's critical GAP catalytic subunit, little is known about its contributions to synaptic function and whether synaptic dysfunction contributes to epilepsy upon loss of *Nprl2*. Previous studies of NPRL2 are limited given that constitutive mouse mutants are lethal due to deficient hematopoiesis and methionine:folate homeostasis (Dutchak et al., 2015). Recent studies with conditional *Nprl2* knockout mice describe that homozygous mutants have mTORC1-dependent seizures, enlarged neurons, and changes in certain metabolites (Hui et al., 2022; Ishida et al., 2021). However, how these alterations might impact synaptic function and how they might contribute to seizure activity has yet to be explored.

To delineate further the role of NPRL2 in epileptogenesis, we have generated a mouse mutant model in which *Nprl2* is conditionally deleted in forebrain excitatory neurons of the neocortex and hippocampus. To provide focus to our study on the cellular level, we have specifically investigated the contributions of mutant neocortical cells. Validating previous studies, mutant mice demonstrate spontaneous seizures and early death by postnatal day (P)21. To investigate the mechanisms driving these severe phenotypes, we have performed histo-pathologic, proteomic, metabolomic, and synaptic electrophysiologic studies. We find that *Nprl2* mutants display marked synaptic dysfunction congruent with network excitability and seizures in these mice. Moreover, we find that mutants also display increased glycine and that glycine's actions on NMDA receptors provide a molecular mechanism contributing to both altered synaptic function and decreased survival phenotypes.

RESULTS

$Emx1^{cre}$; Nprl2 cKO mice have increased mTORC1 activity and spontaneous seizures

Constitutive *Nprl2* mutants display embryonic lethality (Dutchak et al., 2015). Thus, to understand the role of *Nprl2* in the nervous system, we generated a conditional *Nprl2* knockout mouse model by crossing floxed *Nprl2* mice ($Nprl2^{fl/fl}$)(Dutchak et al., 2015) to mice expressing Cre-recombinase driven by the *Emx1* promoter (Gorski et al., 2002). In this model, Cre recombinase is expressed in >80% of the excitatory cells in the neocortex and hippocampus (Gorski et al., 2002). To confirm the specificity of the Cre, an $Emx1^{cre}$; $Nprl2^{fl/+}$ mouse was crossed to a Cre-dependent TdTomato reporter mouse (Madisen et al., 2010) (Figure S1A). We crossed $Nprl2^{fl/fl}$ mice with $Emx1^{cre}$; $Nprl2^{fl/+}$ mice in order to generate control and homozygous (mutant or conditional knockout (cKO)) littermates. Unlike in constitutive *Nprl2* mutants, no embryonic lethality was observed due to preserved Mendelian inheritance ratios (Figure S1B). To verify the deletion of *Nprl2* in the brain, we isolated mouse neocortical tissue and found that *Nprl2* transcripts were significantly reduced compared to controls (Figure S1C). NPRL2 protein levels were also significantly reduced (Figure 1A). The remaining expression is consistent with incomplete recombination in excitatory neurons, together with the lack of recombination and continued expression of *Nprl2* in inhibitory and non-neuronal cells of the brain (Figure 1A). We then examined the impact of *Nprl2* deletion on mTORC1 activity. Because NPRL2 is a negative regulator of mTORC1 activity, we expected *Nprl2* loss to result in increased mTORC1 activity. To assess mTORC1 activity, we measured the amount of phosphorylated ribosomal subunit S6 (pS6). We observed increased pS6 by western blot and immunohistochemistry in mutant neocortical tissue (Figures 1A and 1B).

We then examined whether *Nprl2* loss led to observable changes in the mutant mice and found that mutant body weight was reduced; however, brain weight was significantly increased in the mutants

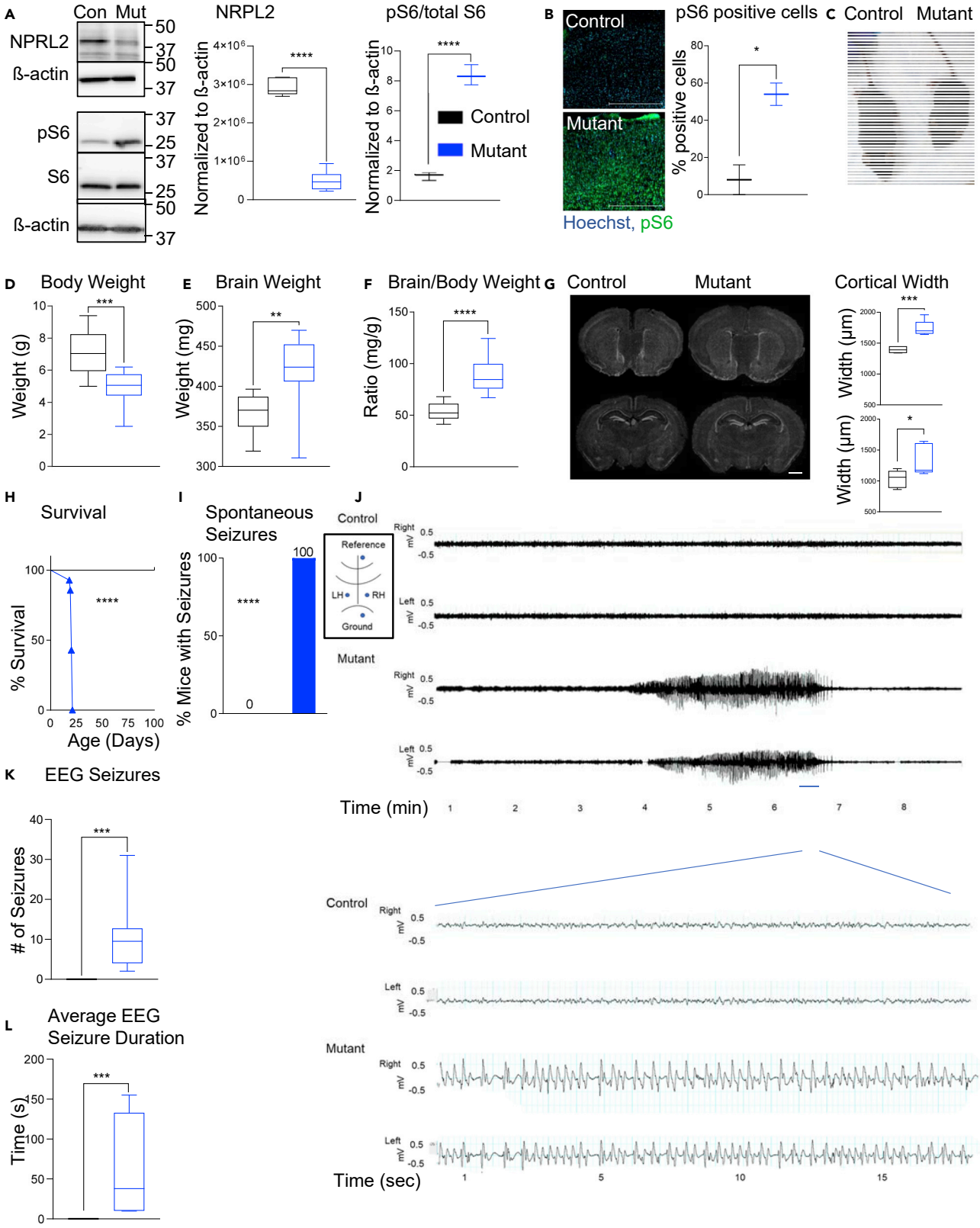
A
Con Mut
NPRL2
ß-actin
pS6
S6
ß-actin
50
37
50
37
37
25
37
25
50
37
NRPL2
Normalized to ß-actin
4×10⁶
3×10⁶
2×10⁶
1×10⁶
0
****
pS6/total S6
Normalized to ß-actin
10
8
6
4
2
0
****
Control
Mutant
B
Control
Mutant
Hoechst, pS6
pS6 positive cells
% positive cells
80
60
40
20
0
*
C
Control
Mutant
D
Body Weight
Weight (g)
10
8
6
4
2
0
***
E
Brain Weight
Weight (mg)
500
450
400
350
300
**
F
Brain/Body Weight
Ratio (mg/g)
150
100
50
0
****
G
Control
Mutant
Cortical Width
Width (µm)
2000
1500
1000
500
***
Width (µm)
2000
1500
1000
500
*
H
Survival
% Survival
100
50
0
****
0 25 50 75 100
Age (Days)
I
Spontaneous Seizures
% Mice with Seizures
100
50
0
****
0
100
J
Control
Reference
LH
RH
Ground
Mutant
Right
Left
0.5
mV
-0.5
Time (min)
1 2 3 4 5 6 7 8
K
EEG Seizures
# of Seizures
40
30
20
10
0
***
L
Average EEG Seizure Duration
Time (s)
200
150
100
50
0
***
Control
Mutant
Right
Left
Time (sec)
1 5 10 15

Figure 1. Emx1^{cre}; *Nprl2* cKO mice have increased mTORC1 activity and spontaneous seizures

(A) Western blot analysis of NPRL2, pS6, and S6 in whole-cell lysates of P16 neocortex. Unpaired two-tailed Student's t test, n = 5 controls, six mutants.

(B) Representative immunohistochemistry for pS6 staining in the neocortex. 10× magnification. Unpaired two-tailed Student's t test, n = 2 controls, two mutants. Scale bar, 500μm.

(C) Representative picture of body size difference, control (left) and mutant (right).

(D–F) Body weight (g), brain weight (mg), and brain/body weight ratio (mg/g) for control and conditional knockout (cKO) mutants. Unpaired two-tailed Student's t test, n = 16 control, nine mutants.

(G) Representative images of Hoechst-stained coronal slices through the neocortex. Control slices (left) and mutant slices (right). Anterior slices (top) and posterior slices (bottom). Scale bar, 1000μm. Unpaired two-tailed Student's t test, n = 5 controls, five mutants (top) six mutants (bottom).

(H) Kaplan-Meier survival curve of control and mutant mice. Mutant mice die by P21. Log rank Mantel Cox test, n = 19 controls, 14 mutants.

(I) Percent of mice that had at least one seizure after handling. Fisher exact test two-sided, n = 20 each genotype.

(J) Representative placement of subdural electrodes. Representative video-EEG paired traces of a seizure in a mutant mouse (trace from control is from corresponding period [no seizures were identified in control mice]). Each trace is from either the right hemisphere (RH) or left hemisphere (LH) of each mouse. Bottom traces are zoomed-in views of period indicated by blue line. n = 7 controls, 8 mutants.

(K) Number of seizures per mouse recorded over 12 h of EEG. Unpaired two-tailed Student's t test, n = 7 controls, 8 mutants.

(L) Average seizure duration per mouse on EEG. Mann-Whitney two-tailed U-test, n = 7 controls, 8 mutants. Whiskers represent minimum to maximum; box represents 25–75 percentile; line represents median. *p < 0.05; **p < 0.01; ***p < 0.001; ****p < 0.0001.

(Figures 1C–1E). Consequently, mutant brain/body weight ratios were significantly increased (Figure 1F). This finding is consistent with models displaying increased mTORC1 activity (Chen et al., 2019; Klofas et al., 2020; Meikle et al., 2008; Yuskaitis et al., 2018). Hoechst staining of brain slices revealed that mutant mice had significantly thicker cortices (Figure 1G), a consistent finding noted with mTORC1 upregulation (Carson et al., 2012; Chen et al., 2019; Ishida et al., 2021; Yuskaitis et al., 2018). In addition to changes in size, mutant mice also demonstrated decreased survival, with no mutants surviving beyond 21 days of age which is similar to other studies (Hui et al., 2022; Ishida et al., 2021) (Figure 1H), while heterozygotes displayed comparable survival to control littermates (data not included).

Because of the association of epilepsy in individuals with *Nprl2* mutations, we examined mice for possible seizure activity. We observed seizure activity, defined as repetitive, tonic-clonic movements, in every mutant examined 1–2 h following handling (Videos S1 and S2). In contrast, no control littermates demonstrated seizure activity (Figure 1I). Out of 20 mutants examined, we observed two mutants die as a direct result of seizure activity. We then performed video-EEG in control and mutant mice at P16-P18. Seizures were identified in all eight mutant mice during 12-h overnight recordings, while no seizures were observed in littermate controls (Figures 1J–1L).

Emx1^{cre}; Nprl2 cKO mice have larger brains, thicker cortical layers, and larger neurons

To understand pathophysiologic mechanisms that might contribute to seizures in mutant mice, we first performed histological analysis to investigate changes caused by loss of *Nprl2* in the neocortex. Because increased brain size and cortical width could be due to increased cell size and/or cell numbers, we measured soma size in pyramidal neurons from layers 2/3 that were filled after recording and found that mutant cells had larger somas compared to littermate controls (Figure S1D). We also utilized automated nuclei counts with ImageJ together with Hoechst staining and found no change in the number of cells in the mouse cortex in mutants compared to controls (Figure S1D). These data point to increased cell size as a primary factor contributing to the enlarged mutant mouse brain.

Given that altered cortical migration can be associated with seizures, we then examined whether cortical lamination might also be impacted. We first stained cortical brain slices with cresyl violet (Figure S1E). To further examine cortical lamination, we stained for CUX1 for upper layers and TBR1 for upper and lower layers (Figure S1F). With the exception of layer 1, which was unchanged in thickness (Figure S1G), we observed thicker cortical layers with TBR1 and CUX1 staining. Lamination of these layers, however, was intact. These data point to normal cortical migration, with changes in the overall appearance likely due to increases in cell size. In addition, mutant mice displayed significantly thicker corpora callosa, which is consistent with larger axonal diameter in a previous model of neuronal mTORC1 upregulation (Ercan et al., 2017) (Figure S1H).

Although *Emx1^{cre}* is expressed in excitatory cells, we also investigated whether loss of *Nprl2* could elicit non-cell autonomous changes. We used antibodies against glutamate decarboxylase 1 isoform 67kD (GAD67) and glial fibrillary acidic protein (GFAP) to stain for inhibitory neurons and astrocytes, respectively.

Inhibitory neuronal numbers were increased in mutant layer 2/3 compared with controls, which may indicate either ectopy as seen in other epilepsy models or a compensatory response to seizure activity (Meikle et al., 2007; Yuskaitis et al., 2018) (Figure S1I). Additionally, we observed increased GFAP signal in astrocytes in the cortex. This increase in GFAP intensity is consistent with reactive astrogliosis as has been shown in multiple models of epilepsy (Carson et al., 2012; Crowell et al., 2015) (Figure S1J). This astrogliosis occurs secondarily to neuronal *Nprl2* loss, as pS6 staining was largely restricted to neurons and did not show any prominent overlap in expression with GFAP similar to other *Nprl2* mouse models (Hui et al., 2022; Ishida et al., 2021) (Figures S1J and S1K).

Emx1^{cre}; Nprl2 cKO mice survival and seizures are rescued by mTORC1 inhibition

We then tested whether the seizures, decreased survival, and brain pathology phenotypes described above in our model are related to NPRL2 regulation of mTORC1 activity. Mice were injected with 6 mg/kg of the mTORC1-specific inhibitor, rapamycin, 3 times a week IP starting at P7 for six weeks (Figure 2A), a dose demonstrated to inhibit mTORC1 in the brain (Meikle et al., 2008). We confirmed that treatment with rapamycin effectively inhibits mTORC1 activity by the observed reduction in pS6 in cortical cells of rapamycin-treated mice (Figures 2B and S2A). Rapamycin treatment caused weight decreases in treated groups as has been demonstrated previously (Chang et al., 2009) (Figure S2B), but it also improved *Nprl2* mutant survival (Figure 2C). In addition, rapamycin significantly rescued seizures in cKO mice. In fact, no seizures were observed in any rapamycin-treated mutants, whereas nearly 50% of vehicle-treated mutants demonstrated seizure activity (Figure 2D). Although we noted a decrease in seizure activity in the vehicle-treated mice compared with untreated animals (Figure 1H), this difference is likely attributable to the shorter period of behavioral observation for these studies (30 min here versus 2 h in the untreated group). To further determine if rapamycin treatment in mutants improved seizures, we recorded video EEG for 12 h in treated P16 pups and found no seizures in any rapamycin-treated mutants out of five tested, whereas all vehicle-treated mutants displayed seizures (Figures 2E, 2F and S2C). Cortical width and brain/body weight ratios were also improved with rapamycin treatment (Figures 2G and S2D). Altogether, these data suggest that seizures, survival, and brain pathology observed in *Emx1^{cre}; Nprl2* mutants are mTORC1-dependent.

Emx1^{cre}; Nprl2 cKO mice layer 2/3 neurons have increased synaptic excitation and decreased inhibition

Synaptic properties play prominent roles in seizures (Du et al., 2019). To investigate potential electrophysiological changes contributing to seizures in mutant mice, we examined synaptic properties in layer 2/3 pyramidal neurons from the cerebral cortex (Figure S3A). We first examined evoked excitatory and inhibitory post synaptic currents. At stimulation strengths that evoked reliable responses, we found a significant increase in the amplitude of evoked excitatory postsynaptic currents (eEPSCs) and a significant decrease in the amplitude of evoked inhibitory postsynaptic currents (eIPSCs) (Figures 3A and 3B).

Resting membrane potential, membrane capacitance, and input resistance were unchanged between control and mutant neurons (Figures S3B–S3D). To examine a potential presynaptic contribution to these findings, we examined release probability using paired pulse ratios. We observed decreased paired-pulse depression in mutant eEPSCs when compared to controls, pointing to increased release probability (Figure 3C). For eIPSCs, we found the opposite, with increased facilitation of the paired-pulse ratio of the eIPSC in mutants, and thus a lower release probability (Figure 3D).

We then examined mini excitatory postsynaptic currents (mEPSCs) and mini inhibitory postsynaptic currents (mIPSCs) from cortical layer 2/3 pyramidal neurons. Mutant cells had no change in amplitude of excitatory currents but showed increased mEPSC frequency when compared to control littermates (Figures 3E–3G). mEPSCs in the mutants also had faster kinetics with quicker rise and decay times (Figures S3E and S3F). To ensure that baseline noise was not contributing to differences in mEPSC detection between groups, we determined root-mean-square baseline noise values and found no differences between genotypes (Figure S3G). Correspondingly, mIPSCs in mutant synapses were also decreased in frequency, yet no change in amplitude was observed (Figures 3H–3I). When we analyzed mIPSC kinetics, the mutants had no change in rise time nor decay time (Figures S3H and S3I). In addition, consistent with these findings, we also observe an increase in the excitatory/inhibitory (E/I) ratio (Figure S3J) We then examined intrinsic cellular excitability and found a reduction in cellular excitability (Figure S3K). Despite this reduction in intrinsic excitability, synaptic function in mutants showed increased excitatory and decreased inhibitory function, consistent with the seizure phenotype demonstrated in *Nprl2* mutant animals.

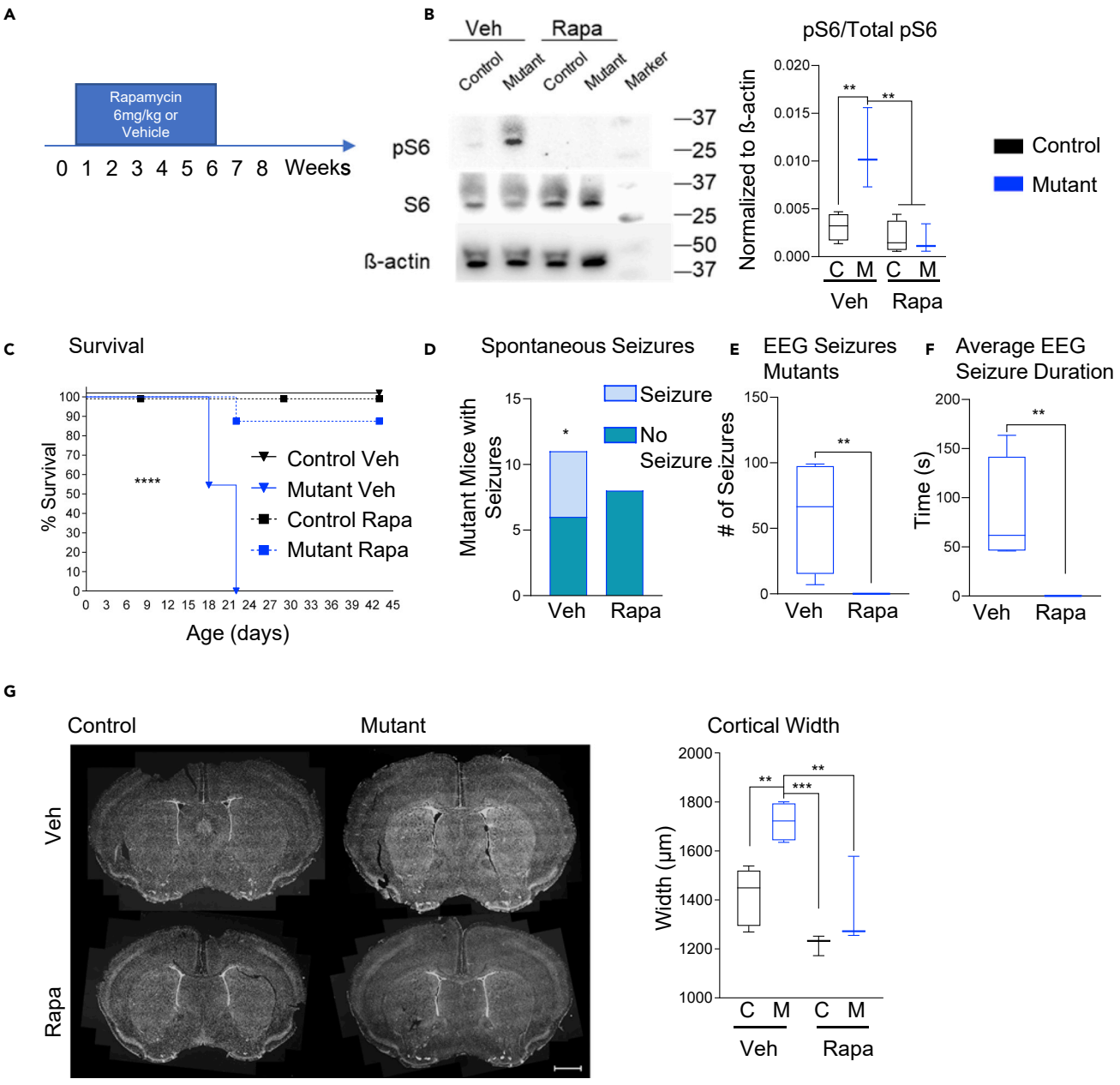

Figure 2. Emx1^{cre}; *Nprl2* cKO mice survival and seizures are rescued by mTOR inhibition

(A) Depiction of rapamycin (rapa) and vehicle (veh) treatments. Mice were treated 3 times a week with either veh or 6 mg/kg rapamycin administered IP.

(B) Western blot analysis of pS6, S6, and β-actin. One-way ANOVA, n = 3 mice per group.

(C) Kaplan-Meier survival curve of control and mutant mice with vehicle treatment or rapamycin treatment. Log rank Mantel-Cox test, n = 7 veh-treated controls, 11 veh-treated mutants, 17 rapa-treated controls, and 8 rapa-treated mutants.

(D) Number of mice observed with seizures during 10- to 20-min period following treatment. Fischer's exact test, two-sided, n = 11 veh-treated mutants, 8 rapa-treated mutants.

(E) Number of seizures per mutant mouse recorded over 12 h of EEG. Mann-Whitney two-tailed U-test, n = 4 veh-treated mutants, 5 rapa-treated mutants.

(F) Average seizure duration per mutant mouse on EEG. Mann-Whitney two-tailed U-test, n = 4 veh-treated mutants, 5 rapa-treated mutants.

(G) Representative images of Hoechst-stained coronal brain slices. One-way ANOVA, n = 5 veh-treated controls, 4 veh-treated mutants, 3 rapa-treated controls, and 3-rapa treated mutants. C = control, M = mutant. Whiskers represent minimum to maximum; box represents 25–75 percentile; line represents median. *p < 0.05; **p < 0.01; ***p < 0.001; ****p < 0.0001.

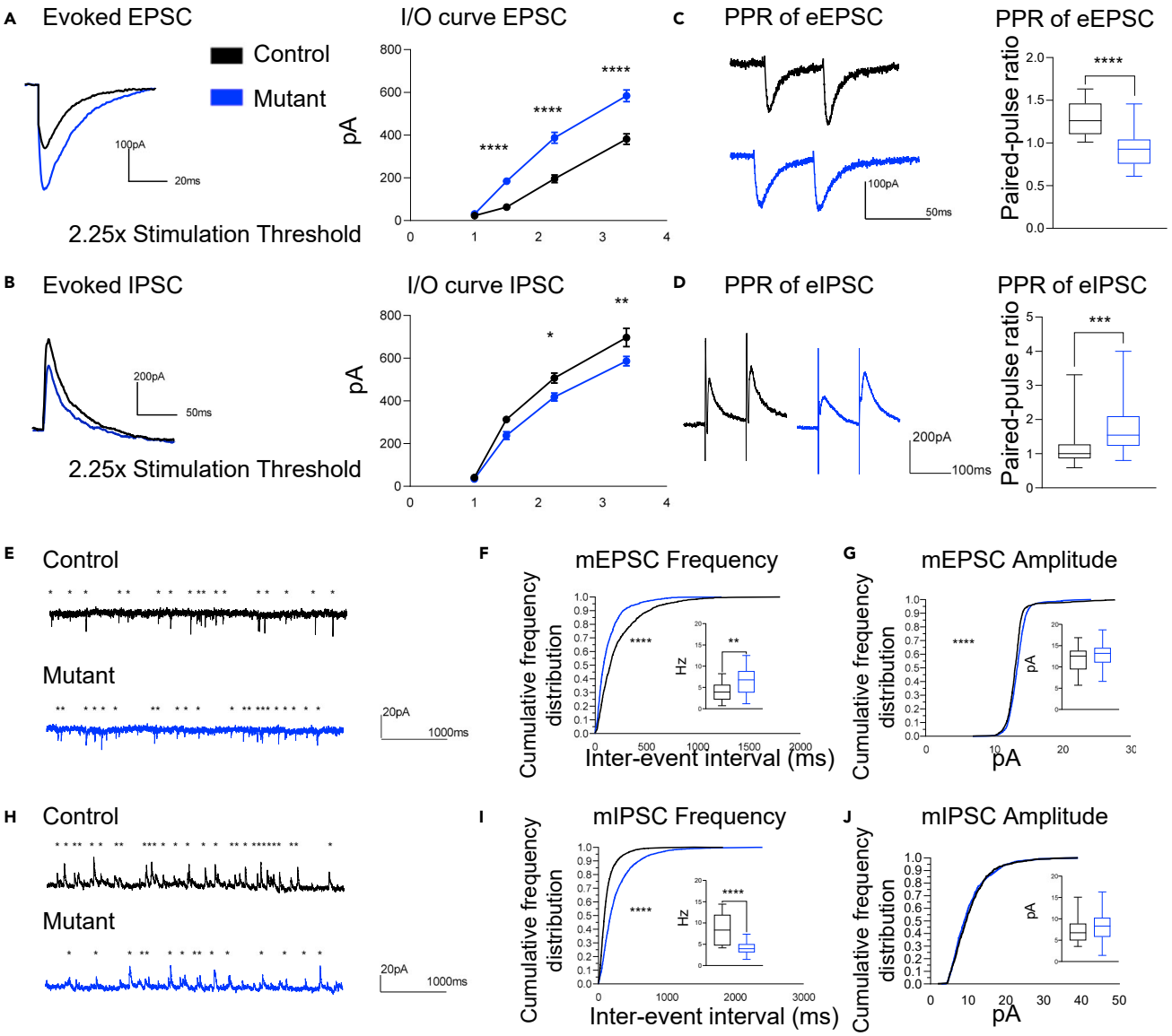

Figure 3. Emx1^{cre}; *Nprl2* cKO mice layer 2/3 neurons have increased synaptic excitation and decreased inhibition

(A) Evoked EPSCs n = 19 cells/6 mice controls, 18 cells/five mice mutants. Representative traces on left; input/output curve on right. two-way ANOVA with Šidák's multiple comparisons.

(B) Evoked IPSCs: n = 26 cells/7 mice controls, 26 cells/6 mice mutants. Representative traces on left; input/output curve on right. two-way ANOVA with Šidák's multiple comparisons.

(C) Representative traces and quantification of paired-pulse ratio (PPR) of eEPSC, 50ms, Unpaired two-tailed Student's t test. n = 21 cells/6 mice each group.

(D) Representative traces and quantification of PPR of eIPSC, 100ms, Unpaired, two-tailed Mann-Whitney U-test. n = 21 cells/6 mice controls, 24 cells/6 mice mutants.

(E) Representative mini (m)EPSC traces.

(F) mEPSC frequency n = 35 cells/11 mice controls, 33 cells/9 mice mutants, and (G) amplitude in control and mutant mice n = 31 cells/11 mice controls, 33 cells/9 mice mutants (H) Representative mini (m)IPSC traces.

(I) mIPSC frequency and (J) amplitude in controls and mutants. n = 21 cells/8 controls, 24 cells/9 mutants. For bar graphs (D, F, G, and J) in this figure, the data did not pass normality test, so we used the Mann-Whitney two-tailed U-test. Cumulative frequency distribution statistical test was Kolmogorov-Smirnov. Asterisks over traces indicate events above threshold. Whiskers represent minimum to maximum; box represents 25–75 percentile; line represents median. *p < 0.05; **p < 0.01; ***p < 0.001; ****p < 0.0001.

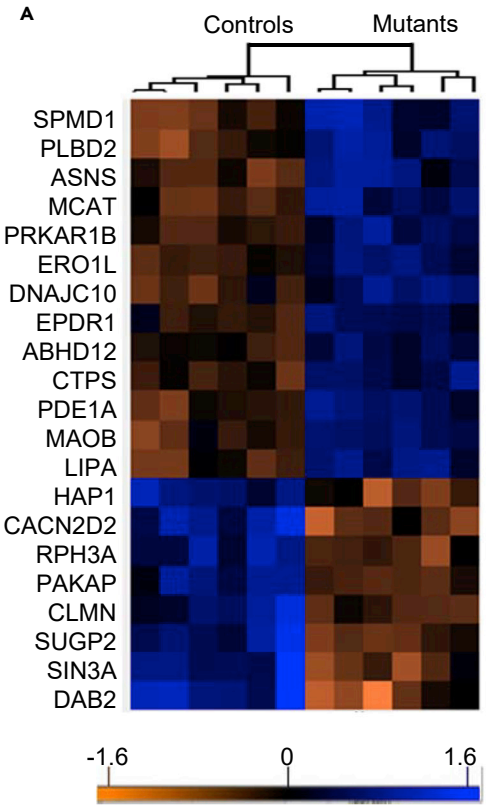

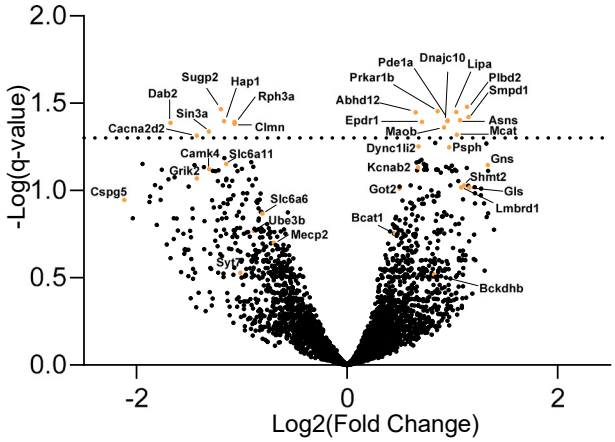

C Significantly (p≤0.05) Altered Epilepsy-Related Proteins

	Up-regulated in mutants	Down-regulated in mutants
Epilepsy associated	SLC25A22, SCARB2	HCN1, PCDH19, SPTAN1
Neurodevelopment associated with epilepsy	NSDHL	UBE3B, SMARCC2, KIF2A, TSC1
Systemic disease associated with epilepsy	SERPINI1, SERPINI1D, PSPH, GBA, ASNS, ABDH12, PSAP,DYNC1LI2, HEXA, NARS, PDHX, CARS, GK, LMAN2, ALDH18A1, AMT, GFAP, IDS, PGK1, PTEN, SACS	GRIK2, MECP2, DNAJC6, SMARCB1, OPLAH, SLC6A11, CHN1, DKC1, IL1RAPL1, MLC1, PDE10A, SNX14
Epilepsy-less known genes	KCNAB2, SYN2, NAPB, SHMT2, BCAT1, BCKDHB, CLNC6, CYB5R1, EIF3E, EXOC6, GBE1, HOMER2, HSD17B7, SEZ6L2, MAOB	CACNA2D2, HAP1, AKT3, L1CAM, PCLB1, CNTN1, PLXNB2, DNM3, HNRNPUL1/2, MAGI2

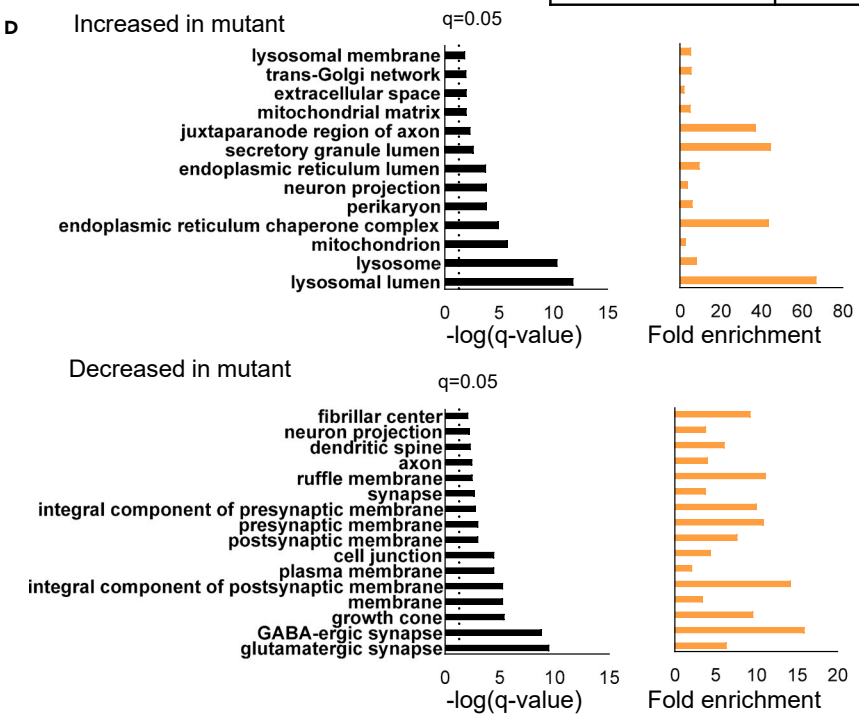

Figure 4. Proteomic analysis reveals downregulated synapse components and altered epilepsy-related proteins

(A) Liquid chromatography-mass spectrometry (LC-MS/MS) heatmap of proteins derived from neocortex. Data were normalized to number of reads in each sample and cluster normalized. Benjamini-Hochberg correction 0.05 cutoff. n = 6 controls and six mutants.

(B) Volcano plot of the data, permutation-based FDR 0.05 cutoff. Highlighted in orange are some of the many epilepsy-related proteins significantly changed by loss of *Nprl2*.

(C) Table of significantly affected epilepsy-related proteins p value $\leq$0.01 cutoff. Orange and bolded indicates q-value $\leq$ 0.05 cutoff.

(D) Up- and downregulated gene ontology cellular component categories. q-values determined by Storey-Tibshirani method.

Proteomic analysis reveals downregulated synapse components and altered epilepsy-related proteins

To determine molecular mechanisms contributing to the abnormal phenotypes seen in cKOs and because the mTORC1 pathway is a major regulator of translation (Jiang et al., 2016; Ma and Blenis, 2009; Wang and Proud, 2006), we investigated relative protein abundance in cortical tissue taken from control and mutant mice with combined liquid chromatography-mass spectrometry (LC-MS/MS) (Figure 4A). We identified changes in numerous proteins, including the downregulation of several epilepsy-related proteins such as CACNA2D2, HAP1, and UBE3B (Figure 4B) (Ambrozkiewicz et al., 2019; Butler et al., 2018; Li et al., 2020).

Epilepsy-related proteins that regulate toxic metabolic accumulations such as NARS, SERPINI1, PSPH, PSAP, ASNS, GBA, GK, and PDHX were all upregulated, which might protect neurons from toxic processes which contribute to seizures. Additionally, numerous metabolic enzymes were upregulated including those involved in aspartate metabolism (GOT1, GOT2, and ASNS), serine anabolism (SHMT2 and PSPH), branched chain amino acid catabolism (BCAT1, BCKDHB, and HIBADH), and glutamine, glycine, and methionine catabolism (GLS, AMT, and MAT2A) (Figure S5D). We adopted the categorization utilized in a recent review of epilepsy-related genes to identify and categorize epilepsy-related proteins that were significantly affected (Wang et al., 2017) (Figure 4C).

We then examined proteins affected with a cutoff of p value less than 0.01 by functional enrichment analysis (Pathan et al., 2015). We found that both proteins involved in glutamatergic and GABAergic synapses were downregulated, while synaptic intermediate filaments and lysosomal proteins were upregulated in mutants (Figure 4D). The proteins affected in the glutamatergic and GABAergic synapse categories are detailed in Table 1(Fukata and Fukata, 2017). *Nprl2* loss led to downregulation of proteins important for neuronal development, synaptogenesis, and dendritic spine formation, all of which can contribute to altered excitatory and inhibitory synaptic function. Additionally, enrichment analysis of molecular function revealed downregulation of proteins that act in GABA reuptake, CaMK cascade phosphorylation, and neurotransmitter binding (Figure S4A). These processes could all lead to decreased synaptic excitation. Biological functions such as GABAergic transmission, neuronal projection, and synapse formation were also decreased after *Nprl2* loss (Figure S4B). Altogether, these findings highlight a crucial role for *Nprl2* in neuronal development, synaptic formation, and the overall excitatory/inhibitory balance in brain activity.

Loss of Nprl2 leads to altered amino acid abundance including increased glycine

Previous research has shown that NPRL2 is involved in regulating cataplerotic reactions related to the TCA cycle (Chen et al., 2017; Laxman et al., 2014), the methionine:folate cycle (Dutchak et al., 2015), and that NPRL2 coordinates glucose and amino acid metabolism in muscle (Dutchak et al., 2018). These metabolic changes are characteristic of inborn errors of metabolism (IEM), which often present with seizures (Almannai and El-Hattab, 2018). To evaluate potential changes in neurotransmitters and metabolic mechanisms that may contribute to decreased survival and seizures, we performed LC-MS/MS with homogenized lysates from the neocortex to quantitate the abundance of over 200 metabolites, with parent/ion ratios listed for some metabolites in Table 2. Significantly altered metabolites were determined with a cutoff FDR q-value of 0.05 (Figures 5A and 5B). As a biological control, cerebellar tissue, where Cre expression and hence recombination of *Nprl2* should be absent, was also analyzed, and no significant metabolite changes were observed in the cerebellum (Figures S5A and S5B). A previous study has demonstrated disruptions in the methionine:folate cycle resulting from *Nprl2* loss (Dutchak et al., 2015). Our data from the neocortex also reflected significant changes in this pathway and showed increases in S-adenosyl-homocysteine (SAH), decarboxylated S-adenosyl methionine (dcSAM), and low methionine, serine, and cystathionine (Figure S5E). Considering the known shunting of amino acids into the TCA cycle in the setting of increased mTORC1 activity (Chen et al., 2017; Dutchak et al., 2015, 2018), we analyzed TCA cycle intermediates and regulators. From these studies, we found that TCA cycle-derived amino acids glutamine and aspartate

Table 1. Downregulated synaptic proteins

Component	Affected Proteins
Glutamatergic Synapse Proteins	ACTN2, ADGRL2, APBA1, ATP2B1, CAMK4, CDH11, CSPG5, DBN1, DNM3, EPHA4, EPS8, FXYD6, GRIK2, LRFN4, LRRC4B, MAGI2, MECP2, NCAM1, NDRG2, NTRK3, PLCB1, PRKCE, PSD2, PTK2B, PTPRS, SYT7
GABAergic Synapse Proteins	SYT7, CAMK4, CSPG5, NLGN2, PLCB1, MAGI2, LRFN4, SLC6A6, ATP2B1, HAP1, SLC6A11

actinin alpha 2 (ACTN2); adhesion G protein-coupled receptor L2 (ADGRL2); amyloid beta (A4) precursor protein binding, family A, member 1 (APBA1); ATPase, Ca++ transporting, plasma membrane 1 (ATP2B1); calcium/calmodulin-dependent protein kinase IV (CAMK4); cadherin 11 (CDH11); chondroitin sulfate proteoglycan 5 (CSPG5); drebrin 1 (DBN1); dynamin 3 (DNM3); Eph receptor A4 (EPHA4); epidermal growth factor receptor pathway substrate 8 (EPS8); FXYD domain-containing ion transport regulator 6 (FXYD6); glutamate receptor, ionotropic, kainate 2 (beta 2) (GRIK2); leucine rich repeat and fibronectin type III domain containing 4 (LRFN4); leucine rich repeat containing 4B (LRRC4B); membrane associated guanylate kinase, WW and PDZ domain containing 2 (MAGI2); methyl CpG binding protein 2 (MECP2); neural cell adhesion molecule 1 (NCAM1); N-myc downstream regulated gene 2 (NDRG2); neurotrophic tyrosine kinase, receptor, type 3 (NTRK3); phospholipase C, beta 1 (PLCB1); protein kinase C, epsilon (PRKCE); pleckstrin and Sec7 domain containing 2 (PSD2); PTK2 protein tyrosine kinase two beta (PTK2B); protein tyrosine phosphatase, receptor type, S (PTPRS); synaptotagmin VII (SYT7); ATPase, Ca++ transporting, plasma membrane 1 (ATP2B1); huntingtin-associated protein 1 (HAP1); neuroligin 2 (NLGN2); solute carrier family 6 (neurotransmitter transporter, GABA), member 11 (SLC6A11); solute carrier family 6 (neurotransmitter transporter, taurine), member 6 (SLC6A6).

were significantly decreased, which is consistent with previous studies in yeast which showed nucleotide synthesis was negatively affected due to decreased amino acid synthesis from TCA cycle intermediates (Figure S5F) (Chen et al., 2017). We also found a subset of amino acids that were significantly decreased in mutants, these included: methionine, serine, threonine, tyrosine, asparagine, glutamine, aspartate, and a trend toward decreased histidine. Glycine, however, was significantly increased (Figure 5C). Glycine can also act as a neurotransmitter, a group of which was also examined given that their availability (Svob Strac et al., 2016) can impact seizure activity. Our data demonstrated trends toward increased dopamine, creatine, melatonin, epinephrine, and choline in *Nprl2* cKO mice (Figure 5D). Putrescine, which acts as an NMDAR co-agonist, was also increased in mutants (Figure S5G). We also observed decreased homovanillic acid (HVA), which is a byproduct of dopamine metabolism. Glutamate and GABA levels, however, were not affected by *Nprl2* loss (Figure 5D).

Increased mEPSCs in Emx1^{cre}; Nprl2 cKO mice result from increased glycine at the NMDA receptor

From our molecular studies, one of the most significantly altered metabolites was the amino acid and neurotransmitter glycine. Consistent with these findings, our proteomic studies highlight a significant increase in SHMT2 (Figure 4), which catalyzes the last enzymatic step in the production of glycine from serine (Figure S5D). Increases in this protein have also been associated with seizure disorders (Escande-Beillard et al., 2020). Hyperglycinergic states have been linked to seizures (nonketotic hyperglycinemia (NKH)) and neurodevelopmental disorders associated with seizures (Escande-Beillard et al., 2020; Iwama et al., 1997; McKenna et al., 2018). Additionally, over the years, there has been increasing evidence for glycine receptor expression in the neocortex of neonatal and adult rodents (McCracken et al., 2017; Naas et al., 1991), and glycine binding both to the glycine receptor and to the glycine$_B$ site on NMDA receptors (NMDARs) (Johnson and Ascher, 1987). We hypothesized that glycine might impact synaptic function and brain network excitability by actions either through the glycine receptor or at the glycine$_B$ site on NMDARs, which has been shown to co-agonize glutamate (Johnson and Ascher, 1987).

We examined whether glycine's binding to the glycine receptor might contribute to network hyperexcitability and seizures. We treated acute slices with the glycine receptor antagonist strychnine. We found no impact on the difference in mEPSC frequency observed between controls and mutants (Figures 6A and 6B) and observed no changes in mEPSC amplitude (Figure S6A). However, mutant mIPSC amplitude was inhibited by strychnine, which provides some evidence of a potentially compensatory, inhibitory influence on mIPSC amplitude likely through strychnine's weak antagonism of GABA-A receptors (Jonas et al., 1998) (Figures S6B–S6D). With application of strychnine, the rise time of mEPSCs was restored to control

Table 2. Parent–daughter ion masses

Metabolites	Parent/Daughter Mass
Serine	106.0/60
Threonine	120/74
Histidine	156.1/110.1
Asparagine	133.1/74
Glycine	76.1/30.5
Methionine	150.1/133
Aspartate	134/74
Glutamine	147.1/84.1
Tyrosine	182.1/77
Sarcosine	89.9/44.1
Sarcosine1	89.9/30.0
GABA-1	103.9/87.0
GABA-2	103.9/45.1
Creatine-1	132.0/90.0
Creatine-2	132.0/44.1
Dopamine-1	154.0/137.0
Dopamine-2	154.0/91.0
Glutamic acid	148.1/84.1
Glutamic acid qualifier	148.1/130.1
Melatonin-1	233.0/174.2
Melatonin-2	233.0/130.0
Norepinephrine-1	170.0/152.0
Norepinephrine-2	170.0/107.1
Serotonin-1	177.0/160.0
Serotonin-2	177.0/115.0
Phosphocreatine-1	211.9/114.0
Phosphocreatine-2	211.9/44.0
Acetylcholine-1	146.0/86.9
Acetylcholine-2	146.0/43.0
5-Hydroxyindole-3-acetic acid	192.2/146.2
Choline	104.3/87.1
Choline qualifier	104.3/69.1
Homovanillic acid	183.2/137.2
Homovanillic acid qualifier	183.2/122
3,4-Dihydroxyphenylacetic acid	183.2/137.2
Arachidonylethanolamide-3	348.1/44.2
Epinephrine-1	184.0/166.1
Epinephrine-2	184.0/106.9

rise time; however, the decay time kinetics of mIPSCs remained increased in mutant mIPSCs despite blockade of the glycine receptor (Figures S6E–S6H).

In addition to glycine's inhibitory actions at its receptor, glycine also binds as an excitatory co-agonist at the glycine$_B$ site on the NMDAR. Strychnine does not affect this glycine co-agonist site on the NMDAR (Johnson and Ascher, 1987). Consistent with a contribution for this NMDAR site to the observed synaptic changes, we also identified a non-significant trend toward decreased kynurenic acid, a factor that inhibits the glycine$_B$ site (Figure S5G). To examine whether increased glycine might contribute to increased

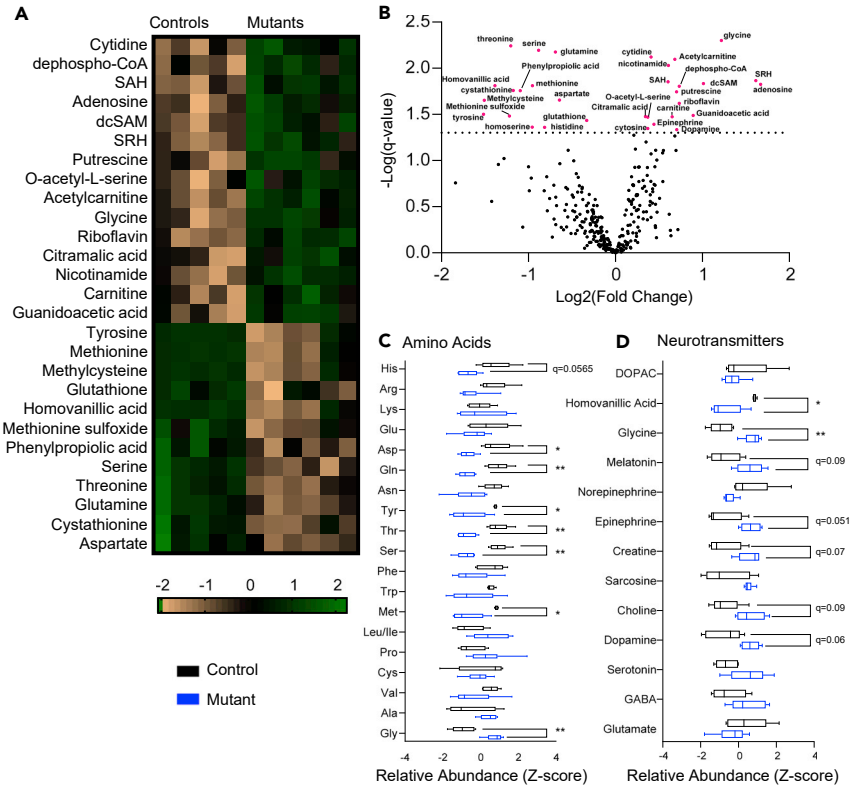

Figure 5. Loss of *Nprl2* leads to altered amino acid abundance including increased glycine

(A) Liquid chromatography-massspectrometry (LC-MS/MS) heatmap of metabolites derived from neocortex. n = 5 controls and 6 mutants. SAH- S-Adenosyl homocysteine, dcSAM- S-Adenosyl methioninamine or decarboxylated S-Adenosyl methionine, SRH- S-Ribosyl homocysteine, 2DG-6-P- 2-dexyglucose-6-phosphate, DOPAC- 3,4 Dihydroxyphenylacetic acid. *Z* score normalized, Student's t test permutation-based FDR q-value<0.05.

(B) Volcano plot of metabolism data, majority of significantly affected metabolites highlighted. Dotted line represents -log(q-value 0.05), Student's t test permutation-based FDR 0.05, q-value <0.05.

(C) Amino acids: *Z* score normalized. Student's t test permutation-based FDR q-value.

(D) Neurotransmitters: *Z* score normalized. Student's t test, permutation-based FDR q-value. Whiskers represent minimum to maximum; box represents 25–75 percentile; line represents median. *q < 0.05; **q < 0.01.

excitatory properties via actions on the NMDAR, we blocked glycine's NMDAR actions with the glycine$_B$ site competitive antagonist 7-chlorokynurenic acid (7-Cl-KYNA). We found that inhibition of the glycine$_B$ site on the NMDAR significantly decreased mEPSC frequency in mutant cells, returning mEPSC frequency to control littermate levels (Figures 6C and 6D) while mEPSC amplitudes remained unaltered (Figure S6I). To examine if this increase in mEPSC was NMDAR-dependent as implicated by these 7-Cl-KYNA studies, we applied R-CPP and found that R-CPP application similarly reduced mEPSC frequency to control levels (Figure S6J). Furthermore, serial application of 7-Cl-KYNA after R-CPP on mutant cells significantly changed the frequency of mEPSCs more than R-CPP alone, consistent with additional KYNA impacts on glutamate release (Grilli et al., 2006; Hilmas et al., 2001; Moroni et al., 2012; Perkins and Stone, 1982; Wang et al., 2006; Wu et al., 2010) (Figure S6K). In further support for an important role of NMDAR blockade in KYNA's effects in *Nprl2* mutant animals, the combined application of CPP and 7-Cl-KYNA demonstrated a significant additive decrease in mutant cell mEPSC frequency compared with the additive impact of 7-Cl-KYNA alone after R-CPP. This further evidences an important role for NMDAR blockade in the 7-Cl-KYNA-mediated improvement of mEPSC frequency in the mutants (Figure S6L). 7-Cl-KYNA also rescued the faster mEPSC kinetics to control littermate levels (Figures S6E and S6F). As a control, blockade of both AMPA and NMDA receptor abolished all excitatory currents (Figure S6M). These findings point to a critical role for glycine actions at the NMDAR in the abnormally increased excitatory properties observed with loss of *Nprl2* (Figures 6C and 6D).

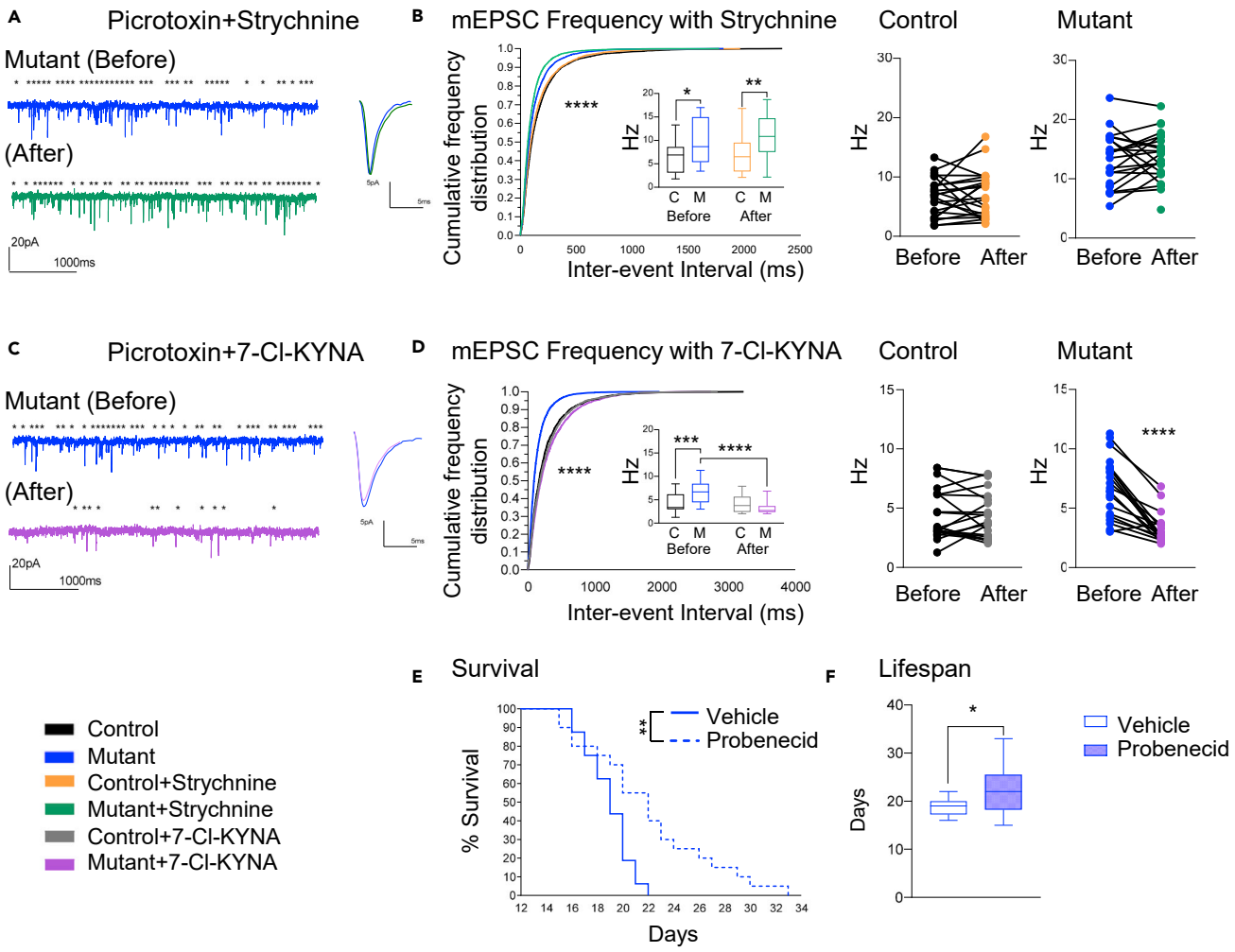

Figure 6. Glycine actions at the NMDA receptor both increases mEPSC frequency and reduces survival in Emx1^{cre}; *Nprl2* cKO mice

(A) Representative mEPSC traces of mutant cells before (top) and after (bottom) strychnine, a blocker of the canonical glycine receptor. Average mEPSC records are shown on right.

(B) mEPSC frequency before and after treatment with strychnine. Cumulative distribution Kruskal-Wallis test, two-way ANOVA with Šidák's multiple comparisons inset graph, before and after application of strychnine frequency for controls (left) and mutants (right), Wilcoxon matched-pairs signed rank two-tailed test. n = 23 cells/7 controls, 23 cells/6 mutants; 23 control cells and 21 mutant cells in before and after graph.

(C) Representative mEPSC traces of mutant cells before (top) and after (bottom) application with 7- Cl-KYNA, a glycine$_B$ blocker. Average mEPSC records are shown on right.

(D) Frequency of mEPSCs with 7-Cl-KYNA treatment. Cumulative distribution Kruskal-Wallis test, two-way ANOVA with Šidák's multiple comparisons inset graph, before and after application of strychnine frequency for controls (left) and mutants (right), Wilcoxon matched-pairs signed rank two-tailed test. n = 23 cells/7 controls, 22 cells/7 mutants; 21 control cells and 18 mutant cells in before and after graph.

(E) Kaplan-Meier survival curve of mutant mice with vehicle (veh) or probenecid treatment. Log rank Mantel Cox test, $p < 0.05$.

(F) Survival of veh-treated and probenecid-treated mutants. Unpaired two-tailed Student's t test; $p < 0.05$, n = 16 veh-treated mutants, 20 probenecid-treated mutants. Asterisks over traces indicate events above threshold. Whiskers represent minimum to maximum; box represents 25–75 percentile; line represents median. *$p < 0.05$; **$p < 0.01$; ***$p < 0.001$; ****$p < 0.0001$.

With these changes in excitatory electrophysiological activity, we then asked whether blockade of the glycine$_B$ site might also improve the survival of *Nprl2* mutant mice which die by P21 (Figure 1H). As noted, kynurenic acid is an endogenous inhibitor of the glycine$_B$ site of the NMDAR. As exogenous kynurenic acid does not efficiently cross the blood–brain barrier, we examined whether the compound probenecid, which increases kynurenic acid levels in the brain by reducing kynurenic acid efflux (Vecsei et al., 1992), would positively impact survival in mutant mice. We administered probenecid to mutant mice starting at P12. We observed significantly improved survival in probenecid-treated mutant mice, with 40% of animals

receiving probenecid surviving beyond P22 compared to 0% in the vehicle-treated cohort (Figures 6E and 6F). Although survival was significantly improved, 50% of the probenecid-treated mutant mice continued to have seizures, which, despite the extension in survival, likely contributed to the continued early mortality in treated mutant mice (Figure S6N).

DISCUSSION

Mice with neuronal *Nprl2* loss in the neocortex and hippocampus develop severe seizures in the first few weeks of life with subsequent death by 21 days of life. These studies provide significant advancements in understanding the synaptic and molecular mechanisms impacted upon *Nprl2* deletion in the cortex and hippocampus of mice. Consistent with other *Nprl2* mouse models, our mutant mice develop severe epilepsy and early death, providing an early survival and seizure endpoint which could prove useful in determining the effectiveness of anti-seizure drug therapies.

Because of the known roles for GATOR1 and NPRL2 in the regulation of mTOR, we then investigated whether phenotypes in mutant mice were mTORC1-dependent. To this end, we treated mutants with the drug rapamycin. Rapamycin and its homologs (rapalogs) have been recommended for medically resistant GATOR1-related epilepsy but are presently approved only for refractory epilepsy related to TSC (Carson et al., 2012; Iffland et al., 2018; Klofas et al., 2020; Yuskaitis et al., 2019). In our model, chronic treatment with rapamycin was successfully able to rescue survival and seizure phenotypes, providing further support for rapalogs as a potential therapy for GATOR1-related epilepsy. However, long-term treatment with rapalogs has serious side effects that often prevent continued use (Franz et al., 2018; Vawter-Lee et al., 2019). Thus, understanding the mechanisms underlying these epilepsies should allow for the discovery of more specific and targeted therapies.

To better understand underlying mechanisms, we sought to evaluate whether synaptic dysfunction might contribute to seizure phenotypes. A previous study (Hui et al., 2022) had looked at intrinsic phenotypes in the lateral habenula, but synaptic changes and intrinsic properties in the cortex have not been previously examined. We observed increased eEPSCs, decreased eIPSCs, and alterations in release probability in layer 2/3 cortical neurons, which point to a presynaptic contribution to these alterations. We also observe increased mEPSC frequency, decreased frequency of mIPSCs along with decreased evoked IPSC amplitude, and an increased excitatory/inhibitory ratio, all of which can promote seizures. Taken together, we identify synaptic changes congruent with the network excitability and seizures observed in these mutant animals.

Paradoxically, intrinsic excitability of these pyramidal cells was found to be decreased, potentially pointing to a compensatory response to the aforementioned synaptic alterations or caused by capacitance changes related to altered cell size. This change in intrinsic excitability observed here differs from a previous report (Hui et al., 2022), with changes potentially emerging from the differences in mutant models examined and in the different brain regions examined for these intrinsic studies.

Loss of *Depdc5* and other models of mTORC1 hyperactivity have shown changes in intrinsic excitability, changes to glutamatergic and GABAergic synapses, and presynaptic changes (De Fusco et al., 2020; Hui et al., 2022; Klofas et al., 2020; Ribierre et al., 2018; Swaminathan et al., 2018; Weston et al., 2014). Our studies, together with previous findings, highlight that GATOR1 loss of function can have wide ranging effects on synaptic function.

To examine potential molecular and metabolic mechanisms driving these synaptic abnormalities, we performed both quantitative proteomic and metabolomic analyses. Glycine was significantly increased in *Nprl2* mutants, as well as enzymes that synthesize (PSPH and SHMT2) glycine and break it down (AMT). Thus, we evaluated whether alterations in glycine contribute to synaptic alterations observed in the mutant. While inhibition of the canonical glycine receptor with strychnine resulted in no significant changes in synaptic properties, our data point to an important contribution of glycine to synaptic excitation that is dependent on the glycine$_B$ site of the NMDAR. After blocking the glycine$_B$ site at the NMDAR with a selective inhibitor of this site, 7-KYNA (Kleckner and Dingledine, 1989), we found a significant decrease in mEPSC frequency. This change mirrors the decrease in mEPSC frequency elicited by blocking the NMDAR with R-CPP, which together demonstrates an important excitatory role for the excess of glycine. As mEPSCs are mediated by AMPAR, these findings point to NMDAR-dependent effects upstream of these synapses,

which is consistent with previous studies demonstrating glycine effects on presynaptic role and further consistent with known presynaptic glycine actions on the NMDARs (Li and Han, 2007). We also show increases in release probability for eEPSCs, consistent with this presynaptic mechanism.

We then asked whether we could target this mechanism *in vivo* in *Nprl2* mutants. Treatment with the organic acid transport inhibitor, probenecid, which inhibits efflux of kynurenic acid, (as noted above, an NMDAR glycine$_B$ site inhibitor) resulted in a significant improvement in survival in our mutant mice. This result is consistent with a critical role for this mechanism in the severe mutant phenotypes, although we cannot completely exclude a potential benefit derived from a generalized reduction in excitatory transmission with probenecid treatment. Taken together, however, these findings highlight the therapeutic potential of targeting the NMDAR and specifically the glycine$_B$ site on the NMDAR. Despite improvement in survival, mutant mice still developed seizures while on probenecid treatment, which likely relates to the modest impact of probenecid on KYNA levels. Methods to increase KYNA levels or target the NMDAR at this site are presently being investigated for several different disorders (Wu et al., 2005; Zanos et al., 2015) and might offer additional improvements to those observed in this study. Furthermore, the glycine$_B$ site and increases in glycine have been implicated in other epilepsies and neurodevelopmental disorders (Allen et al., 2013; Swanger et al., 2016) such as TSC, in which patients also develop intellectual disability and autism-related deficits (Almannai and El-Hattab, 2018; Escande-Beillard et al., 2020; McKenna et al., 2018). In addition, kynurenic acid has been implicated in a number of neurodevelopmental disorders and autism (Bryn et al., 2017; Gevi et al., 2016; Iwama et al., 1997; Matsuo et al., 1995). Thus, pharmacologic treatment at this site could provide a therapeutic avenue for several disorders.

Our proteomic and metabolomic analyses reveal not only significant upregulation of glycine but also multiple additional altered metabolites that may contribute to seizure phenotypes in mutant animals. First, we have found many alterations in epilepsy-linked proteins. Some were changed in directions consistent with genetic epilepsies, while some protein changes appear opposite, suggestive of a potential compensatory response to the loss of *Nprl2*. For instance, many of the epilepsy-related upregulated proteins are enzymes that process metabolites and, when dysfunctional, lead to toxic accumulations or metabolic deficiencies that are implicated in epilepsy (Ben-Salem et al., 2015; Ranza et al., 2017; Tonin et al., 2019). Many of these proteins are, however, increased in mutant mice, a finding that may reflect a homeostatic mechanism to accommodate for increased mTORC1 activity and resulting disruption of cellular processes. Epilepsy-related proteins that were decreased included HAP1 and UBE3B, both involved in clearance systems (Ambrozkiewicz et al., 2019; Basel-Vanagaite et al., 2012; Li et al., 2020; Wang et al., 2019).

Although metabolic changes after neuronal *Nprl2* loss have been explored (Hui et al., 2022), we found some overlap but also significant differences in the amino acids and neurotransmitters that were significantly changed. Differences in results could be due to specific aspects of differing methodology and could also be attributed to different mouse models. Nonetheless, our methodology allowed us to test for an extensive panel of amino acids, neurotransmitters, and other metabolites within the neocortex and the cerebellum, a control brain region without *Nprl2* deletion. In our studies, we focus on glycine, given its important roles as a neurotransmitter. Our metabolomics analyses showed a substantial overlap with our proteomics results, specifically identifying pathways associated with amino acid anabolism and catabolism. These changes are often implicated in inborn errors of metabolism (IEMs), which present high rates of seizures and metabolic disturbances (Figure S5D). In addition to the elevated glycine, we found low serine, altered one-carbon metabolism, and high guanidoacetic acid (GAA) (Almannai and El-Hattab, 2018). Glycine, serine, threonine, and methionine metabolism are intricately linked and have all been implicated in seizure development (de Koning and Klomp, 2004). Also, in our proteomic studies, phosphoserine phosphatase (PSPH) and mitochondrial serine hydroxymethyltransferase (SHMT2) are upregulated in the mutants. These proteins promote the synthesis of glycine and L-serine and could potentially offer a therapeutic target to reduce glycine. Methionine is also significantly decreased in our mutant mice, which is known to impact the SAM:SAH ratio in cells and has been associated with seizures (Perry et al., 2008). Furthermore, vitamin B12 is an essential co-factor to one-carbon metabolism and its deficiency in infants can promote seizures (Benbir et al., 2007). Loss of *Nprl2* can impact the processing of this vitamin (Dutchak et al., 2015), which is consistent with the altered one-carbon metabolism in our mutant mice. Similarly, accumulation of GAA together with GAMT deficiency can impact creatine synthesis, another pathway-associated seizures (Almannai and El-Hattab, 2018; de Koning and Klomp, 2004; Neu et al., 2002). Notably, amino acid synthesis and catabolism can also impact neurotransmitter metabolism. Although in our mutant data many

Table 3. KickqStart™ qPCR Primers, related to STAR Methods

Species	Gene	Gene ID	Primer Pair
Mouse	*Nprl2*	56032	1
Mouse	*Gfap*	14580	1
Mouse	*Th*	21823	1
Mouse	*Maob*	109731	1
Mouse	*Drd1a*	13488	1
Mouse	*Drd2*	13489	1
Mouse	*Ddc*	13195	1
Mouse	*Slc6a8*	102857	1
Mouse	*Gamt*	14431	1
Mouse	*Gatn (Agat)*	67092	1
Mouse	*Comt*	12846	1
Mouse	*Mthfr*	17769	1

neuromodulatory neurotransmitters trended toward a significant increase, GABA and glutamate remained unchanged. Nonetheless, we have evidence that dopaminergic signaling is significantly affected with the combined results of proteomics (increased MAOB), qRT-PCR (decreased *Drd1a*, *Drd2, Th, Maob,* and *Ddc*) (Figure S5C, Table 3) and metabolomics (trending toward increased dopamine, decreased homovanillic acid (HVA)) analyses. Dopamine signaling and the mTOR pathway have been associated in previous studies, while alterations in this neurotransmitter can lead to epilepsy (Svob Strac et al., 2016).

In this study, we have generated $Emx1^{cre};Nprl2^{fl/fl}$ mutant mice, which display a severe seizure phenotype and markedly reduced survival. We demonstrate that this loss of *Nprl2* disrupts synaptic transmission through glycine signaling at the NMDAR, resulting in increased synaptic excitation. Targeting this mechanism both normalizes excitatory synaptic abnormalities and improves survival. This model also provides a high-altitude view of other potential contributing proteomic and metabolic mechanisms that are important avenues of future study. Further investigation of this mouse model thus may not only illuminate other causative and potentially therapeutically targetable mechanisms that underlie the pathogenesis of *Nprl2* loss-related seizures but may also shed light on and contribute to treatment related to modulation of the $glycine_B$ site for both mTORC1-related and unrelated epilepsies.

Limitations of the study

In our study, we focused primarily on the effects of *Nprl2* loss in the cerebral cortex, specifically in excitatory neurons. Hippocampal cells were also affected in our model; however, we have not yet investigated their contribution to our phenotypes. Given the known implications of the hippocampus to epilepsy, it is possible that it contributes to the seizures and decreased survival of our mutant mice. Thus, it will be important to investigate this aspect in future studies. Furthermore, with loss of *Nprl2*, we find significant decreases in synaptic inhibition along with increased number of inhibitory cells in layers 2/3 of the cortex. These changes in inhibitory function could result from the affected excitatory neurons or through non-cell autonomous effects of inhibitory neurons or glia. Given that *Nprl2* is expressed in all cell types of the brain, follow-up studies in other neurons or glia could reveal additional roles for the GATOR complex. Finally, a caveat of our study is that we were not able to sufficiently evaluate behavioral deficits as a consequence of *Nprl2* loss, given decreased survival of the mutant mice. Alternative models will be needed to explore the contribution of NPRL2 and GATOR1 components to behaviors commonly impacted in NDDs.

STAR★METHODS

Detailed methods are provided in the online version of this paper and include the following:

- KEY RESOURCES TABLE
- RESOURCE AVAILABILITY
  - Lead contact
  - Materials availability
  - Data and code availability

SUPPLEMENTAL INFORMATION

Supplemental information can be found online at https://doi.org/10.1016/j.isci.2022.104334.

ACKNOWLEDGMENTS

Dr. Paul Dutchak for providing the *Nprl2*$^{fl/fl}$ mouse. Hamid Baniasadi for expertise in metabolomics. UT Southwestern Proteomics Core and Dr. Andrew Lemoff. UT Southwestern Live Cell Imaging Facility. UT Southwestern Neuro Models Facility- Dr. Erik Plautz. UT Southwestern Whole Brain Microscopy Facility. Jennifer Gibson for expertise and assistance in *in vivo* experiments. B.P.T. acknowledges CPRIT RP140655 and R01 NS115546. P.T.T. acknowledges DOD W81XWH-17-1-0238 and institutional startup funds.

AUTHOR CONTRIBUTIONS

Conceptualization, B.D., L.A.P., B.P.T., and P.T.T.; Methodology, B.D., L.A.P., V.J., A.J.H., B.P.T., and P.T.T.; Investigation, B.D., L.A.P., C.R., V.J., A.J.H., D.C., E.O., and K.M.H.; Graphical Abstract, V.J.; Writing – Original Draft, B.D. and P.T.T.; Writing – Review & Editing, B.D., L.A.P., V.J., J.M.P., and P.T.T.

DECLARATION OF INTERESTS

The authors declare no competing interests.

INCLUSION AND DIVERSITY

One or more of the authors of this paper self-identifies as an underrepresented ethnic minority in science.

Received: December 22, 2020
Revised: September 16, 2021
Accepted: April 26, 2022
Published: May 20, 2022

REFERENCES

Allen, A.S., Berkovic, S.F., Cossette, P., Delanty, N., Dlugos, D., Eichler, E.E., Epstein, M.P., Glauser, T., Goldstein, D.B., Han, Y., et al. (2013). De novo mutations in epileptic encephalopathies. Nature *501*, 217–221. https://doi.org/10.1038/nature12439.

Almannai, M., and El-Hattab, A.W. (2018). Inborn errors of metabolism with seizures. Pediatr. Clin. North Am. *65*, 279–299. https://doi.org/10.1016/j.pcl.2017.11.007.

Ambrozkiewicz, M.C., Ripamonti, S., Borisova, E., Schwark, M., Schaub, T., Altas, B., Yilmaz, R., Piepkorn, L., Horan, S., Jahn, O., et al. (2019). The Kaufman oculocerebrofacial syndrome protein Ube3b regulates synapse number by ubiquitinating Ppp3cc. Preprint at bioRxiv. https://doi.org/10.1101/672923.

Baldassari, S., Licchetta, L., Tinuper, P., Bisulli, F., and Pippucci, T. (2016). GATOR1 complex: the common genetic actor in focal epilepsies. J. Med. Genet. *53*, 503–510. https://doi.org/10.1136/jmedgenet-2016-103883.

Baldassari, S., Picard, F., Verbeek, N.E., van Kempen, M., Brilstra, E.H., Lesca, G., Conti, V., Guerrini, R., Bisulli, F., Licchetta, L., et al. (2019). The landscape of epilepsy-related GATOR1 variants. Genet. Med. *21*, 398–408. https://doi.org/10.1038/s41436-018-0060-2.

Bar-Peled, L., Chantranupong, L., Cherniack, A.D., Chen, W.W., Ottina, K.A., Grabiner, B.C., Spear, E.D., Carter, S.L., Meyerson, M., and Sabatini, D.M. (2013). A Tumor suppressor complex with GAP activity for the Rag GTPases that signal amino acid sufficiency to mTORC1. Science *340*, 1100–1106. https://doi.org/10.1126/science.1232044.

Basel-Vanagaite, L., Dallapiccola, B., Ramirez-Solis, R., Segref, A., Thiele, H., Edwards, A., Arends, M.J., Miró, X., White, J.K., Désir, J., et al.

(2012). Deficiency for the ubiquitin ligase UBE3B in a blepharophimosis-ptosis-intellectual-disability syndrome. Am. J. Hum. Genet. *91*, 998–1010. https://doi.org/10.1016/j.ajhg.2012.10.011.

Ben-Salem, S., Gleeson, J.G., Al-Shamsi, A.M., Islam, B., Hertecant, J., Ali, B.R., and Al-Gazali, L. (2015). Asparagine synthetase deficiency detected by whole exome sequencing causes congenital microcephaly, epileptic encephalopathy and psychomotor delay. Metab. Brain Dis. *30*, 687–694. https://doi.org/10.1007/s11011-014-9618-0.

Benbir, G., Uysal, S., Saltik, S., Zeybek, C.A., Aydin, A., Dervent, A., and Yalcinkaya, C. (2007). Seizures during treatment of Vitamin B12 deficiency. Seizure *16*, 69–73. https://doi.org/10.1016/j.seizure.2006.10.016.

Bryn, V., Verkerk, R., Skjeldal, O.H., Saugstad, O.D., and Ormstad, H. (2017). Kynurenine pathway in autism spectrum disorders in children. Neuropsychobiology *76*, 82–88. https://doi.org/10.1159/000488157.

Butler, K.M., Holt, P.J., Milla, S.S., da Silva, C., Alexander, J.J., and Escayg, A. (2018). Epileptic encephalopathy and cerebellar atrophy resulting from compound heterozygous CACNA2D2 variants. Case Rep. Genet. *2018*, 6308283. https://doi.org/10.1155/2018/6308283.

Carson, R.P., Van Nielen, D.L., Winzenburger, P.A., and Ess, K.C. (2012). Neuronal and glia abnormalities in Tsc1-deficient forebrain and partial rescue by rapamycin. Neurobiol. Dis. *45*, 369–380. https://doi.org/10.1016/j.nbd.2011.08.024.

Chang, G.R., Wu, Y.Y., Chiu, Y.S., Chen, W.Y., Liao, J.W., Hsu, H.M., Chao, T.H., Hung, S.W., and Mao, F.C. (2009). Long-term administration of rapamycin reduces adiposity, but impairs glucose tolerance in high-fat diet-fed KK/HlJ mice. Basic Clin. Pharmacol. Toxicol. *105*, 188–198. https://doi.org/10.1111/j.1742-7843.2009.00427.x.

Chen, C.J., Sgritta, M., Mays, J., Zhou, H., Lucero, R., Park, J., Wang, I.C., Park, J.H., Kaipparettu, B.A., Stoica, L., et al. (2019). Therapeutic inhibition of mTORC2 rescues the behavioral and neurophysiological abnormalities associated with Pten-deficiency. Nat. Med. *25*, 1684–1690. https://doi.org/10.1038/s41591-019-0608-y.

Chen, J., Sutter, B.M., Shi, L., and Tu, B.P. (2017). GATOR1 regulates nitrogenic cataplerotic reactions of the mitochondrial TCA cycle. Nat. Chem. Biol. *13*, 1179–1186. https://doi.org/10.1038/nchembio.2478.

Cho, K.O., Lybrand, Z.R., Ito, N., Brulet, R., Tafacory, F., Zhang, L., Good, L., Ure, K., Kernie, S.G., Birnbaum, S.G., et al. (2015). Aberrant hippocampal neurogenesis contributes to epilepsy and associated cognitive decline. Nat. Commun. *6*, 6606. https://doi.org/10.1038/ncomms7606.

Crino, P.B. (2015). mTOR signaling in epilepsy: insights from malformations of cortical development. Cold Spring Harb. Perspect. Med. *5*, a022442. https://doi.org/10.1101/cshperspect.a022442.

Crowell, B., Hwa Lee, G., Nikolaeva, I., Dal Pozzo, V., and D'Arcangelo, G. (2015). Complex neurological phenotype in mutant mice lacking *Tsc2* in excitatory neurons of the developing forebrain. eNeuro *2*. ENEURO.0046-0015.2015. https://doi.org/10.1523/ENEURO.0046-15.2015.

de Calbiac, H., Dabacan, A., Marsan, E., Tostivint, H., Devienne, G., Ishida, S., Leguern, E., Baulac, S., Muresan, R.C., Kabashi, E., and Ciura, S. (2018). Depdc5 knockdown causes mTOR-dependent motor hyperactivity in zebrafish. Ann. Clin. Transl. Neurol. *5*, 510–523. https://doi.org/10.1002/acn3.542.

De Fusco, A., Cerullo, M.S., Marte, A., Michetti, C., Romei, A., Castroflorio, E., Baulac, S., and Benfenati, F. (2020). Acute knockdown of Depdc5 leads to synaptic defects in mTOR-related epileptogenesis. Neurobiol. Dis. *139*, 104822. https://doi.org/10.1016/j.nbd.2020.104822.

de Koning, T.J., and Klomp, L.W. (2004). Serine-deficiency syndromes. Curr. Opin. Neurol. *17*, 197–204. https://doi.org/10.1097/00019052-200404000-00019.

Dibbens, L.M., de Vries, B., Donatello, S., Heron, S.E., Hodgson, B.L., Chintawar, S., Crompton, D.E., Hughes, J.N., Bellows, S.T., Klein, K.M., et al. (2013). Mutations in DEPDC5 cause familial focal epilepsy with variable foci. Nat. Genet. *45*, 546–551. https://doi.org/10.1038/ng.2599.

Dokudovskaya, S., and Rout, M.P. (2015). SEA you later alli-GATOR–a dynamic regulator of the TORC1 stress response pathway. J. Cell Sci. *128*, 2219–2228. https://doi.org/10.1242/jcs.168922.

Dokudovskaya, S., Waharte, F., Schlessinger, A., Pieper, U., Devos, D.P., Cristea, I.M., Williams, R., Salamero, J., Chait, B.T., Sali, A., et al. (2011). A conserved coatomer-related complex containing Sec13 and Seh1 dynamically associates with the vacuole in Saccharomyces cerevisiae. Mol. Cell. Proteomics *10*. M110.006478. https://doi.org/10.1074/mcp.M110.006478.

Du, J., Vegh, V., and Reutens, D.C. (2019). Small changes in synaptic gain lead to seizure-like activity in neuronal network at criticality. Sci. Rep. *9*, 1097. https://doi.org/10.1038/s41598-018-37646-9.

Dutchak, P.A., Estill-Terpack, S.J., Plec, A.A., Zhao, X., Yang, C., Chen, J., Ko, B., Deberardinis, R.J., Yu, Y., and Tu, B.P. (2018). Loss of a negative regulator of mTORC1 induces aerobic glycolysis and altered fiber composition in skeletal muscle. Cell Rep. *23*, 1907–1914. https://doi.org/10.1016/j.celrep.2018.04.058.

Dutchak, P.A., Laxman, S., Estill, S.J., Wang, C., Wang, Y., Wang, Y., Bulut, G.B., Gao, J., Huang, L.J., and Tu, B.P. (2015). Regulation of hematopoiesis and methionine homeostasis by mTORC1 inhibitor NPRL2. Cell Rep. *12*, 371–379. https://doi.org/10.1016/j.celrep.2015.06.042.

Düvel, K., Yecies, J.L., Menon, S., Raman, P., Lipovsky, A.I., Souza, A.L., Triantafellow, E., Ma, Q., Gorski, R., Cleaver, S., et al. (2010). Activation of a metabolic gene regulatory network downstream of mTOR complex 1. Mol. Cell *39*, 171–183. https://doi.org/10.1016/j.molcel.2010.06.022.

Ercan, E., Han, J.M., Di Nardo, A., Winden, K., Han, M.J., Hoyo, L., Saffari, A., Leask, A., Geschwind, D.H., and Sahin, M. (2017). Neuronal CTGF/CCN2 negatively regulates myelination in a mouse model of tuberous sclerosis complex. J. Exp. Med. *214*, 681–697. https://doi.org/10.1084/jem.20160446.

Escande-Beillard, N., Loh, A., Saleem, S.N., Kanata, K., Hashimoto, Y., Altunoglu, U., Metoska, A., Grandjean, J., Ng, F.M., Pomp, O., et al. (2020). Loss of PYCR2 causes neurodegeneration by increasing cerebral Glycine levels via SHMT2. Neuron *107*, 82–94.e6. https://doi.org/10.1016/j.neuron.2020.03.028.

Franz, D.N., Lawson, J.A., Yapici, Z., Ikeda, H., Polster, T., Nabbout, R., Curatolo, P., de Vries, P.J., Dlugos, D.J., Voi, M., et al. (2018). Everolimus for treatment-refractory seizures in TSC: extension of a randomized controlled trial. Neurol. Clin. Pract. *8*, 412–420. https://doi.org/10.1212/cpj.0000000000000514.

Fukata, Y., and Fukata, M. (2017). Epilepsy and synaptic proteins. Curr. Opin. Neurobiol. *45*, 1–8. https://doi.org/10.1016/j.conb.2017.02.001.

Gevi, F., Zolla, L., Gabriele, S., and Persico, A.M. (2016). Urinary metabolomics of young Italian autistic children supports abnormal tryptophan and purine metabolism. Mol. Autism *7*, 47. https://doi.org/10.1186/s13229-016-0109-5.

Gorski, J.A., Talley, T., Qiu, M., Puelles, L., Rubenstein, J.L.R., and Jones, K.R. (2002). Cortical excitatory neurons and glia, but not GABAergic neurons, are produced in the Emx1-expressing lineage. J. Neurosci. *22*, 6309–6314. https://doi.org/10.1523/jneurosci.22-15-06309.2002.

Grilli, M., Raiteri, L., Patti, L., Parodi, M., Robino, F., Raiteri, M., and Marchi, M. (2006). Modulation of the function of presynaptic α7 and non-α7 nicotinic receptors by the tryptophan metabolites, 5-hydroxyindole and kynurenate in mouse brain. Br. J. Pharmacol. *149*, 724–732. https://doi.org/10.1038/sj.bjp.0706914.

Hilmas, C., Pereira, E.F.R., Alkondon, M., Rassoulpour, A., Schwarcz, R., and Albuquerque, E.X. (2001). The brain metabolite kynurenic acid inhibits α7 nicotinic receptor activity and increases non-α7 nicotinic receptor expression: physiopathological implications. J. Neurosci. *21*, 7463–7473. https://doi.org/10.1523/jneurosci.21-19-07463.2001.

Holz, M.K., Ballif, B.A., Gygi, S.P., and Blenis, J. (2005). mTOR and S6K1 mediate assembly of the translation preinitiation complex through dynamic protein interchange and ordered phosphorylation events. Cell *123*, 569–580. https://doi.org/10.1016/j.cell.2005.10.024.

Hui, J.B., Silva, J.C.H., Pelaez, M.C., Sévigny, M., Venkatasubramani, J.P., Plumereau, Q., Chahine, M., Proulx, C.D., Sephton, C.F., and Dutchak, P.A. (2022). NPRL2 inhibition of mTORC1 controls sodium channel expression and brain amino acid homeostasis. eNeuro *9*. ENEURO.0317-21.2022. https://doi.org/10.1523/eneuro.0317-21.2022.

Iffland, P.H., 2nd, Baybis, M., Barnes, A.E., Leventer, R.J., Lockhart, P.J., and Crino, P.B. (2018). DEPDC5 and NPRL3 modulate cell size, filopodial outgrowth, and localization of mTOR in neural progenitor cells and neurons. Neurobiol. Dis. *114*, 184–193. https://doi.org/10.1016/j.nbd.2018.02.013.

Ishida, S., Zhao, D., Sawada, Y., Hiraoka, Y., Mashimo, T., and Tanaka, K. (2021). Dorsal telencephalon-specific Nprl2- and

Nprl3-knockout mice: novel mouse models for GATORopathy. Hum. Mol. Genet. ddab337. https://doi.org/10.1093/hmg/ddab337.

Iwama, H., Takahashi, K., Kure, S., Hayashi, F., Narisawa, K., Tada, K., Mizoguchi, M., Takashima, S., Tomita, U., and Nishikawa, T. (1997). Depletion of cerebral D-serine in non-ketotic hyperglycinemia: possible involvement of glycine cleavage system in control of endogenous D-serine. Biochem. Biophys. Res. Commun. *231*, 793–796. https://doi.org/10.1006/bbrc.1997.6184.

Jiang, X., Feng, S., Chen, Y., Feng, Y., and Deng, H. (2016). Proteomic analysis of mTOR inhibition-mediated phosphorylation changes in ribosomal proteins and eukaryotic translation initiation factors. Protein Cell *7*, 533–537. https://doi.org/10.1007/s13238-016-0279-0.

Johnson, J.W., and Ascher, P. (1987). Glycine potentiates the NMDA response in cultured mouse brain neurons. Nature *325*, 529–531. https://doi.org/10.1038/325529a0.

Jonas, P., Bischofberger, J., and Sandkühler, J. (1998). Corelease of two fast neurotransmitters at a central synapse. Science *281*, 419–424. https://doi.org/10.1126/science.281.5375.419.

Kim, J., Kundu, M., Viollet, B., and Guan, K.L. (2011). AMPK and mTOR regulate autophagy through direct phosphorylation of Ulk1. Nat. Cell Biol. *13*, 132–141. https://doi.org/10.1038/ncb2152.

Kim, J.K., and Lee, J.H. (2019). Mechanistic target of rapamycin pathway in epileptic disorders. J. Korean Neurosurg. Soc. *62*, 272–287. https://doi.org/10.3340/jkns.2019.0027.

Kleckner, N.W., and Dingledine, R. (1989). Selectivity of quinoxalines and kynurenines as antagonists of the glycine site on N-methyl-D-aspartate receptors. Mol. Pharmacol. *36*, 430–436.

Klofas, L.K., Short, B.P., Zhou, C., and Carson, R.P. (2020). Prevention of premature death and seizures in a Depdc5 mouse epilepsy model through inhibition of mTORC1. Hum. Mol. Genet. *29*, 1365–1377. https://doi.org/10.1093/hmg/ddaa068.

Lasarge, C.L., and Danzer, S.C. (2014). Mechanisms regulating neuronal excitability and seizure development following mTOR pathway hyperactivation. Front. Mol. Neurosci. *7*, 18. https://doi.org/10.3389/fnmol.2014.00018.

Laxman, S., Sutter, B.M., Shi, L., and Tu, B.P. (2014). Npr2 inhibits TORC1 to prevent inappropriate utilization of glutamine for biosynthesis of nitrogen-containing metabolites. Sci. Signal. *7*, ra120. https://doi.org/10.1126/scisignal.2005948.

Li, R., Wu, B., He, M., Zhang, P., Zhang, Q., Deng, J., Yuan, J., and Chen, Y. (2020). HAP1 modulates epileptic seizures by regulating GABA(A)R function in patients with temporal lobe epilepsy and in the PTZ-induced epileptic model. Neurochem. Res. *45*, 1997–2008. https://doi.org/10.1007/s11064-020-03052-9.

Li, Y.H., and Han, T.Z. (2007). Glycine binding sites of presynaptic NMDA receptors may tonically regulate glutamate release in the rat visual cortex. J. Neurophysiol. *97*, 817–823. https://doi.org/10.1152/jn.00980.2006.

Lipton, J.O., and Sahin, M. (2014). The Neurology of mTOR. Neuron *84*, 275–291. https://doi.org/10.1016/j.neuron.2014.09.034.

Ma, X.M., and Blenis, J. (2009). Molecular mechanisms of mTOR-mediated translational control. Nat. Rev. Mol. Cell Biol. *10*, 307–318. https://doi.org/10.1038/nrm2672.

Ma, X.M., Yoon, S.O., Richardson, C.J., Jülich, K., and Blenis, J. (2008). SKAR links pre-mRNA splicing to mTOR/S6K1-mediated enhanced translation efficiency of spliced mRNAs. Cell *133*, 303–313. https://doi.org/10.1016/j.cell.2008.02.031.

Madisen, L., Zwingman, T.A., Sunkin, S.M., Oh, S.W., Zariwala, H.A., Gu, H., Ng, L.L., Palmiter, R.D., Hawrylycz, M.J., Jones, A.R., et al. (2010). A robust and high-throughput Cre reporting and characterization system for the whole mouse brain. Nat. Neurosci. *13*, 133–140. https://doi.org/10.1038/nn.2467.

Marsan, E., and Baulac, S. (2018). Review: mechanistic target of rapamycin (mTOR) pathway, focal cortical dysplasia and epilepsy. Neuropathol. Appl. Neurobiol. *44*, 6–17. https://doi.org/10.1111/nan.12463.

Matsuo, S., Inoue, F., Takeuchi, Y., Yoshioka, H., Kinugasa, A., and Sawada, T. (1995). Efficacy of tryptophan for the treatment of nonketotic hyperglycinemia: a new therapeutic approach for modulating the N-methyl-D-aspartate receptor. Pediatrics *95*, 142–146. https://doi.org/10.1542/peds.95.1.142.

McCracken, L.M., Lowes, D.C., Salling, M.C., Carreau-Vollmer, C., Odean, N.N., Blednov, Y.A., Betz, H., Harris, R.A., and Harrison, N.L. (2017). Glycine receptor α3 and α2 subunits mediate tonic and exogenous agonist-induced currents in forebrain. Proc. Natl. Acad. Sci. U S A *114*, E7179–E7186. https://doi.org/10.1073/pnas.1703839114.

McKenna, J., 3rd, Kapfhamer, D., Kinchen, J.M., Wasek, B., Dunworth, M., Murray-Stewart, T., Bottiglieri, T., Casero, R.A., Jr., and Gambello, M.J. (2018). Metabolomic studies identify changes in transmethylation and polyamine metabolism in a brain-specific mouse model of tuberous sclerosis complex. Hum. Mol. Genet. *27*, 2113–2124. https://doi.org/10.1093/hmg/ddy118.

Meikle, L., Pollizzi, K., Egnor, A., Kramvis, I., Lane, H., Sahin, M., and Kwiatkowski, D.J. (2008). Response of a neuronal model of tuberous sclerosis to mammalian target of rapamycin (mTOR) inhibitors: effects on mTORC1 and Akt signaling lead to improved survival and function. J. Neurosci. *28*, 5422–5432. https://doi.org/10.1523/jneurosci.0955-08.2008.

Meikle, L., Talos, D.M., Onda, H., Pollizzi, K., Rotenberg, A., Sahin, M., Jensen, F.E., and Kwiatkowski, D.J. (2007). A mouse model of tuberous sclerosis: neuronal loss of Tsc1 causes dysplastic and ectopic neurons, reduced myelination, seizure activity, and limited survival. J. Neurosci. *27*, 5546–5558. https://doi.org/10.1523/jneurosci.5540-06.2007.

Moloney, P.B., Cavalleri, G.L., and Delanty, N. (2021). Epilepsy in the mTORopathies: opportunities for precision medicine. Brain Commun. *3*, fcab222. https://doi.org/10.1093/braincomms/fcab222.

Moroni, F., Cozzi, A., Sili, M., and Mannaioni, G. (2012). Kynurenic acid: a metabolite with multiple actions and multiple targets in brain and periphery. J. Neural Transm. *119*, 133–139. https://doi.org/10.1007/s00702-011-0763-x.

Naas, E., Zilles, K., Gnahn, H., Betz, H., Becker, C.M., and Schröder, H. (1991). Glycine receptor immunoreactivity in rat and human cerebral cortex. Brain Res. *561*, 139–146. https://doi.org/10.1016/0006-8993(91)90758-n.

Neu, A., Neuhoff, H., Trube, G., Fehr, S., Ullrich, K., Roeper, J., and Isbrandt, D. (2002). Activation of GABA(A) receptors by guanidinoacetate: a novel pathophysiological mechanism. Neurobiol. Dis. *11*, 298–307. https://doi.org/10.1006/nbdi.2002.0547.

Panchaud, N., Peli-Gulli, M.P., and De Virgilio, C. (2013). Amino acid deprivation inhibits TORC1 through a GTPase-activating protein complex for the Rag family GTPase Gtr1. Sci. Signal. *6*, ra42. https://doi.org/10.1126/scisignal.2004112.

Pathan, M., Keerthikumar, S., Ang, C.S., Gangoda, L., Quek, C.Y., Williamson, N.A., Mouradov, D., Sieber, O.M., Simpson, R.J., Salim, A., et al. (2015). FunRich: an open access standalone functional enrichment and interaction network analysis tool. Proteomics *15*, 2597–2601. https://doi.org/10.1002/pmic.201400515.

Perkins, M.N., and Stone, T.W. (1982). An iontophoretic investigation of the actions of convulsant kynurenines and their interaction with the endogenous excitant quinolinic acid. Brain Res. *247*, 184–187. https://doi.org/10.1016/0006-8993(82)91048-4.

Perry, S., Levasseur, J., Chan, A., and Shea, T.B. (2008). Dietary supplementation with S-adenosyl methionine was associated with protracted reduction of seizures in a line of transgenic mice. Comp. Med. *58*, 604–606.

Ranza, E., Garcia-Tarodo, S., Varvagiannis, K., Guipponi, M., Lobrinus, J.A., Bottani, A., Kern, I., Kurian, M., Pittet, M.P., Antonarakis, S.E., et al. (2017). SERPINI1 pathogenic variants: an emerging cause of childhood-onset progressive myoclonic epilepsy. Am. J. Med. Genet. A *173*, 2456–2460. https://doi.org/10.1002/ajmg.a.38317.

Ribierre, T., Deleuze, C., Bacq, A., Baldassari, S., Marsan, E., Chipaux, M., Muraca, G., Roussel, D., Navarro, V., Leguern, E., et al. (2018). Second-hit mosaic mutation in mTORC1 repressor DEPDC5 causes focal cortical dysplasia-associated epilepsy. J. Clin. Invest. *128*, 2452–2458. https://doi.org/10.1172/jci99384.

Ricos, M.G., Hodgson, B.L., Pippucci, T., Saidin, A., Ong, Y.S., Heron, S.E., Licchetta, L., Bisulli, F., Bayly, M.A., Hughes, J., et al.; Epilepsy Electroclinical Study Group (2016). Mutations in the mammalian target of rapamycin pathway regulators NPRL2 and NPRL3 cause focal epilepsy. Ann. Neurol. *79*, 120–131. https://doi.org/10.1002/ana.24547.

Shen, K., Valenstein, M.L., Gu, X., and Sabatini, D.M. (2019). Arg78 of Nprl2 catalyzes GATOR1-stimulated GTP hydrolysis by the rag GTPases.

J. Biol. Chem. *294*, 2970–5944. https://doi.org/10.1074/jbc.AC119.007382.

Sutter, B.M., Wu, X., Laxman, S., and Tu, B.P. (2013). Methionine inhibits autophagy and promotes growth by inducing the SAM-responsive methylation of PP2A. Cell *154*, 403–415. https://doi.org/10.1016/j.cell.2013.06.041.

Svob Strac, D., Pivac, N., Smolders, I.J., Fogel, W.A., De Deurwaerdere, P., and Di Giovanni, G. (2016). Monoaminergic mechanisms in epilepsy may offer innovative therapeutic opportunity for monoaminergic multi-target drugs. Front. Neurosci. *10*, 492. https://doi.org/10.3389/fnins.2016.00492.

Swaminathan, A., Hassan-Abdi, R., Renault, S., Siekierska, A., Riche, R., Liao, M., de Witte, P.A.M., Yanicostas, C., Soussi-Yanicostas, N., Drapeau, P., et al. (2018). Non-canonical mTOR-independent role of DEPDC5 in regulating GABAergic network development. Curr. Biol. *28*, 1924–1937.e5. https://doi.org/10.1016/j.cub.2018.04.061.

Swanger, S.A., Chen, W., Wells, G., Burger, P.B., Tankovic, A., Bhattacharya, S., Strong, K.L., Hu, C., Kusumoto, H., Zhang, J., et al. (2016). Mechanistic insight into NMDA receptor dysregulation by rare variants in the GluN2A and GluN2B agonist binding domains. Am. J. Hum. Genet. *99*, 1261–1280. https://doi.org/10.1016/j.ajhg.2016.10.002.

Tatebe, H., and Shiozaki, K. (2017). Evolutionary conservation of the components in the TOR signaling pathways. Biomolecules *7*, 77. https://doi.org/10.3390/biom7040077.

Tonin, R., Catarzi, S., Caciotti, A., Procopio, E., Marini, C., Guerrini, R., and Morrone, A. (2019). Progressive myoclonus epilepsy in Gaucher Disease due to a new Gly-Gly mutation causing loss of an Exonic Splicing Enhancer. J. Neurol. *266*, 92–101. https://doi.org/10.1007/s00415-018-9084-4.

Tsai, P.T., Hull, C., Chu, Y., Greene-Colozzi, E., Sadowski, A.R., Leech, J.M., Steinberg, J., Crawley, J.N., Regehr, W.G., and Sahin, M. (2012). Autistic-like behaviour and cerebellar dysfunction in Purkinje cell Tsc1 mutant mice. Nature *488*, 647–651. https://doi.org/10.1038/nature11310.

Tyanova, S., Temu, T., Sinitcyn, P., Carlson, A., Hein, M.Y., Geiger, T., Mann, M., and Cox, J. (2016). The Perseus computational platform for comprehensive analysis of (prote)omics data. Nat. Methods *13*, 731–740. https://doi.org/10.1038/nmeth.3901.

Vawter-Lee, M., Franz, D.N., Fuller, C.E., and Greiner, H.M. (2019). Clinical Letter: a case report of targeted therapy with sirolimus for NPRL3 epilepsy. Seizure *73*, 43–45. https://doi.org/10.1016/j.seizure.2019.10.007.

Vecsei, L., Miller, J., MacGarvey, U., and Flint Beal, M. (1992). Kynurenine and probenecid inhibit pentylenetetrazol- and NMDLA-induced seizures and increase kynurenic acid concentrations in the brain. Brain Res. Bull. *28*, 233–238. https://doi.org/10.1016/0361-9230(92)90184-y.

Wang, J., Lin, Z.J., Liu, L., Xu, H.Q., Shi, Y.W., Yi, Y.H., He, N., and Liao, W.P. (2017). Epilepsy-associated genes. Seizure *44*, 11–20. https://doi.org/10.1016/j.seizure.2016.11.030.

Wang, J., Simonavicius, N., Wu, X., Swaminath, G., Reagan, J., Tian, H., and Ling, L. (2006). Kynurenic acid as a ligand for orphan G protein-coupled receptor GPR35. J. Biol. Chem. *281*, 22021–22028. https://doi.org/10.1074/jbc.M603503200.

Wang, T., Wang, J., Wang, J., Mao, L., Tang, B., Vanderklish, P.W., Liao, X., Xiong, Z.Q., and Liao, L. (2019). HAP1 is an in vivo UBE3A target that augments autophagy in a mouse model of Angelman syndrome. Neurobiol. Dis. *132*, 104585. https://doi.org/10.1016/j.nbd.2019.104585.

Wang, X., and Proud, C.G. (2006). The mTOR pathway in the control of protein synthesis. Physiology (Bethesda, Md) *21*, 362–369. https://doi.org/10.1152/physiol.00024.2006.

Weckhuysen, S., Marsan, E., Lambrecq, V., Marchal, C., Morin-Brureau, M., An-Gourfinkel, I., Baulac, M., Fohlen, M., Kallay Zetchi, C., Seeck, M., et al. (2016). Involvement of GATOR complex genes in familial focal epilepsies and focal cortical dysplasia. Epilepsia *57*, 994–1003. https://doi.org/10.1111/epi.13391.

Weston, M.C., Chen, H., and Swann, J.W. (2014). Loss of mTOR repressors Tsc1 or Pten has divergent effects on excitatory and inhibitory synaptic transmission in single hippocampal neuron cultures. Front. Mol. Neurosci. *7*, 1. https://doi.org/10.3389/fnmol.2014.00001.

Wojnicz, A., Avendano Ortiz, J., Casas, A.I., Freitas, A.E., G López, M., and Ruiz-Nuno, A. (2016). Simultaneous determination of 8 neurotransmitters and their metabolite levels in rat brain using liquid chromatography in tandem with mass spectrometry: application to the murine Nrf2 model of depression. Clinica Chim. Acta Int. J. Clin. Chem. *453*, 174–181. https://doi.org/10.1016/j.cca.2015.12.023.

Wu, H.Q., Pereira, E.F.R., Bruno, J.P., Pellicciari, R., Albuquerque, E.X., and Schwarcz, R. (2010). The astrocyte-derived α7 nicotinic receptor antagonist kynurenic acid controls extracellular glutamate levels in the prefrontal cortex. J. Mol. Neurosci. *40*, 204–210. https://doi.org/10.1007/s12031-009-9235-2.

Wu, H.Q., Rassoulpour, A., Goodman, J.H., Scharfman, H.E., Bertram, E.H., and Schwarcz, R. (2005). Kynurenate and 7-chlorokynurenate formation in chronically epileptic rats. Epilepsia *46*, 1010–1016. https://doi.org/10.1111/j.1528-1167.2005.67404.x.

Wu, X., and Tu, B.P. (2011). Selective regulation of autophagy by the Iml1-Npr2-Npr3 complex in the absence of nitrogen starvation. Mol. Biol. Cell *22*, 4124–4133. https://doi.org/10.1091/mbc.E11-06-0525.

Yuskaitis, C.J., Jones, B.M., Wolfson, R.L., Super, C.E., Dhamne, S.C., Rotenberg, A., Sabatini, D.M., Sahin, M., and Poduri, A. (2018). A mouse model of DEPDC5-related epilepsy: neuronal loss of Depdc5 causes dysplastic and ectopic neurons, increased mTOR signaling, and seizure susceptibility. Neurobiol. Dis. *111*, 91–101. https://doi.org/10.1016/j.nbd.2017.12.010.

Yuskaitis, C.J., Rossitto, L.A., Gurnani, S., Bainbridge, E., Poduri, A., and Sahin, M. (2019). Chronic mTORC1 inhibition rescues behavioral and biochemical deficits resulting from neuronal Depdc5 loss in mice. Hum. Mol. Genet. *28*, 2952–2964. https://doi.org/10.1093/hmg/ddz123.

Zanos, P., Piantadosi, S.C., Wu, H.Q., Pribut, H.J., Dell, M.J., Can, A., Snodgrass, H.R., Zarate, C.A., Jr., Schwarcz, R., and Gould, T.D. (2015). The prodrug 4-chlorokynurenine causes Ketamine-like antidepressant effects, but not side effects, by NMDA/GlycineB-Site inhibition. J. Pharmacol. Exp. Ther. *355*, 76–85. https://doi.org/10.1124/jpet.115.225664.

STAR★METHODS

KEY RESOURCES TABLE

REAGENT or RESOURCE	SOURCE	IDENTIFIER
Antibodies		
Mouse monoclonal NPRL2 (F-3)	Santa Cruz	sc-376986; NA
Rabbit monoclonal phospho-S6 (Ser235/236)	Cell Signaling	cat#4858S; RRID:AB_916156
Rabbit monoclonal S6	Cell Signaling	cat#2217; RRID:AB_331355
Mouse monoclonal beta-actin	Sigma-Aldrich	Cat# A2228; RRID:AB_476697
Rat monoclonal GFAP	ThermoFisher	Cat#13-0300; RRID:AB_2532994
Rabbit polyclonal CUX1	Proteintech	Cat#11733-1-AP; RRID:AB_2086995
Rabbit monoclonal TBR1	Abcam	Cat# AB31940; RRID:AB_2200219
Mouse monoclonal GAD67	Millipore	Cat# MAB5406; RRID:AB_2278725
Alexa Fluor® 488 Streptavidin	Jackson Immunoresearch	Cat# 016-540-084; RRID:AB_2337249
Chemicals, Peptides, and Recombinant Proteins		
Rapamycin	LC-Labs	R-5000
Probenecid	Sigma	P8761
NBQX	Sigma	N183
Picrotoxin	Tocris	1128
Strychnine	Sigma	S0532
Neurobiotin tracer	Vector Laboratories	SP-1120
TTX	Abcam	AB120054
R-CPP	Tocris	0247/10
7-Cl-KYNA	Tocris	0237
Critical Commercial Assays		
Pierce BCA Assay	Thermo Fisher	23225
RNEasy Mini Kit	Qiagen	74104
iScript™ Reverse Transcription Supermix	Bio-Rad	1708841
Deposited Data		
Raw Proteomics data	This manuscript	MassIVE: MSV000088098
Raw Metabolomics data	This manuscript	MetaboLights: MTBLS4676
Experimental Models: Organisms/Strains		
Nprl2 floxed mice	Dr. Paul Dutchak; (Dutchak et al., 2015)	NA
Emx1^{cre} mice (B6.129S2-*Emx1*$^{tm1(cre)Krj}$ /J)	The Jackson Laboratory	IMSR_JAX:005628
TdTomato Cre Reporter mice (B6.Cg-*Gt(ROSA) 26Sor*$^{tm14(CAG-tdTomato)Hze}$/J)	The Jackson Laboratory	IMSR_JAX:007914
Oligonucleotides		
Nprl2 F-genotyping: CTCAGGTTCTACGCA GTGACTTC	Dutchak et al., 2015	N/A
Nprl2 R- genotyping: CATGGCGCTGTCT GGATCC	Dutchak et al., 2015	N/A
Nprl2 KO- genotyping: CAGGCTTCATAC TTCTACCCTC	Dutchak et al., 2015	N/A
Emx1 RBGipAdirect1- genotyping: GTATT TGGTTTAGAGTTTGGC	Kevin Jones, University of Colorado	N/A

(*Continued on next page*)

Continued

REAGENT or RESOURCE	SOURCE	IDENTIFIER
Emx1 3′UTR- genotyping: GGGG GACATGAGAGGATGTCAC	Kevin Jones, University of Colorado	N/A
Emx1 EmxPCrDirect3- genotyping: GTGC CATCATGAAGGATGC	Kevin Jones, University of Colorado	N/A
Primers for qRTPCR see Table 3		N/A
Software and Algorithms		
ImageJ	NIH	https://imagej.net/ RRID:SCR_003070
PRISM	Graphpad 9.3.1.471	https://www.graphpad.com/scientific-software/prism/
Perseus	Max Planck Institute of Biochemistry	http://www.perseus-framework.org RRID:SCR_015753
FunRich: Functional Enrichment analysis tool	Pathan et al., 2015 (*Proteomics*)	http://www.funrich.org/ RRID:SCR_014467
MatLab	MathWorks R2020b	http://www.mathworkm.com/products/matlma/ RRID:SCR_001622
Image Lab	Bio-Rad 6.1	http://www.bio-rad.com/en-us/sku/1709690-image-lab-software RRID:SCR_014210
Zen lite	Zeiss 6.2.9200.0	https://www.zeiss.coc/microscopy/us/proprodu/microscope-software/zen-lite.html RRID:SCR_018163
NanoZoomer Digital Pathology	Hamamatsu	https://www.hamamatsu.com/us/en/product/type/U12388-01/index.html
LabChart 8 Reader	ADInstruments 8.1.18	https://www.adinstruadins.com/products/labchart RRID:SCR_017551
MultiQuant 3.0.3	SciEx	https://sciex.com/products/software/multiquant-software
Proteome Discoverer 2.2	Thermo Fisher	https://www.thermofisher.com/order/catalog/product/IQLAAEGABSFAKJMAUH RRID:SCR_014477
pClamp 10	Axon Instruments	http://www.moleculermolecul.com/productp/software/pclamp.htht RRID:SCR_011323
easy_electrophysiology 2.3.2		https://www.easyelectrophysiology.com/

RESOURCE AVAILABILITY

Lead contact

Further information and requests for resources and reagents should be directed to and will be fulfilled by the lead contact, Peter T. Tsai (peter.tsai@utsouthwestern.edu)

Materials availability

This study did not generate new unique reagents. Mouse lines used in this study will be made available on request.

Data and code availability

Proteomics data has been uploaded to the MassIVE database and are publicly available as of the date of publication. Accession numbers are listed in the key resources table.

Metabolomics data has been uploaded to the MetaboLights database and are publicly available as of the date of publication. Accession numbers are listed in the key resources table.

This paper does not report original code.

Any additional information required to reanalyze the data reported in this paper is available from the lead contact upon request.

EXPERIMENTAL MODEL AND SUBJECT DETAILS

Emx1-cre (*Emx1^{cre}*) transgenic mice were obtained from Jackson Laboratories (Gorski et al., 2002). Conditional knockout (cKO) mutant animals, *Emx1^{cre}; Nprl2$^{fl/fl}$* mice, were generated by crossing *Emx1^{cre}* transgenic mice with mice possessing loxP-flanked *Nprl2* (Dutchak et al., 2015). *Emx1^{cre}; Nprl2$^{fl/+}$* mice were crossed to *Nprl2$^{fl/fl}$* mice to generate mutants, heterozygotes, and control littermates. Genotyping PCR primers for *Nprl2:* Forward: 5′-CTCAGGTTCTACGCAGTGACTTC; Reverse: 5′-CATGGCGCTGTCTG GATCC; KO: 5′ CAGGCTTCATACTTCTACCCTC. *Emx1^{cre}* specific primers: RBGipAdirect1: 5′-GTATT TGGTTTAGAGTTTGGC-3′; Emx3′UTR: 5′-GGGGGACATGAGAGGATGTCAC-3′; EmxPCrDirect3: 5′-GT GCCATCATGAAGGATGC-3′. Littermate controls were used in all behavioral experiments. Male and female mice were used in all experiments and allocated to experimental groups randomly, based on genotype. All experimental protocols were approved by UT Southwestern's Institutional Animal Care and Use Committee.

METHOD DETAILS

Western blots

To quantify protein levels, cell lysates were prepared from neocortex taken from Postnatal day (P)16-18 mice. To ensure similar protein amount were loaded, samples were quantified with Pierce™ BCA Protein assay. Gels were loaded with 30μg per well in 10% SDS polyacrylamide gels. Primary antibodies utilized: mouse-NPRL2 (Santa Cruz, sc-376986), rabbit-phospho-S6 (Ser235/236) (Cell Signaling, cat#4858S), rabbit-S6 (Cell Signaling, cat#2217), mouse-beta actin (Sigma-Aldrich, Cat# A2228). To detect the primary antibodies, the following horseradish peroxidase-conjugated antibodies were used: goat anti-rabbit HRP secondary antibody (Azure Biosystems, AC2114), goat anti-mouse HRP secondary antibody (Azure biosystems, AC2115). HRP was detected via application of Clarity™ Western ECL Substrate (Bio-Rad), and imaged with ChemiDoc imager (Bio-Rad). Blots were stripped and re-blotted for S6 and β-actin. Fresh stripping buffer was prepared with solution of 200mM Glycine, 0.1% SDS, 1% Tween 20, dissolved in distilled water, pH adjusted to 2.2 with HCl. Membrane was incubated twice with stripping buffer 5 minutes each, then washed in 1x PBS twice 10 minutes each, then washed in TBST twice for 5 minutes each, then blocked in BSA. Densitometric analysis was performed using Image Lab software, bands were normalized to β-actin signal in each sample.

Immunohistochemistry

Mice were perfused on P16-P18, and the extracted brains were fixed in 4% paraformaldehyde overnight. Brains were switched to 30% sucrose in PBS the following day. 30μm coronal slices were cut using a freezing microtome. Slices were stained as floating sections following standard protocols. Aldehydes were quenched with a 0.3M Glycine solution before staining. Primary antibodies utilized were rabbit-pS6 (Ser235/236) (Cell Signaling, cat#4858S), rat-GFAP (ThermoFisher, 13-0300), rabbit-CUX1(Proteintech, 11733-1-AP), rabbit-TBR1(Abcam, AB31940), mouse-GAD67(Millipore, MAB5406). Primary antibodies were detected with the following secondary antibodies: goat anti-mouse 488 (Invitrogen A-11001), goat anti-mouse 594 (Invitrogen A-11005), goat anti-rabbit 488 (Invitrogen A-11008), goat anti-rabbit 594 (Invitrogen A-11012), goat anti-rat 594 (Invitrogen A-11007). Nuclei were stained with Hoechst 33342. Stained brain slices were imaged on Zeiss Axioscan Z1, or Zeiss Axioscope.A1 Upright Fluorescence Microscope in UT Southwestern's Whole Brain Microscopy Facility. Images were analyzed on Zen-lite software. Cell number was quantified using ImageJ within a defined region of interest.

Neurobiotin-filled cells in 300μm thick coronal slices were stained with Alexa Fluor® 488 Streptavidin (Jackson Immunoresearch, 016-540-084). Nuclei were stained with Hoechst 33342. Cells were imaged on Zeiss LSM 780 Inverted Confocal Microscope at the UT Southwestern Live Cell Imaging Facility. Cell soma area was measured using ImageJ.

Immunohistochemistry analysis

For all measurements, comparable frontal brain slices between the control, mutant, untreated and treated mice were analyzed.

For pS6 quantification, we selected a region of interest within Layer 2/3 of the cortex. Total number of cells within the region of interest was determined using Hoechst 33342 staining. From Hoechst 33342 positive

cells, we quantified all cells with green (Alexa 488) fluorescence that surpassed background brightness (determined with Zen Lite).

For cortical thickness and corpus callosum measurements, Hoechst staining was used to label all cell nuclei. Zen Lite was used to draw a line from the outer edge of Layer 1 of the cortex to Layer 6 in one brain hemisphere. This line was later measured in microns. For the corpus callosum, the distance was measured within the corpus callosum, in the middle of both brain hemispheres. Refer to Figure S1H for line placement and representative images. Measurements from three sections and both hemispheres were averaged for each mouse and graphed.

Regarding CUX1 and TBR1 measurements, immunofluorescence in upper or lower cortical layers was used as a reference. On both brain hemispheres, a line was drawn to include all layers in which cells had significant fluorescence compared to background. For TBR1, only the lower cortical layers were measured. Measurements from three sections and both hemispheres were averaged for each mouse and graphed.

For Layer 1 measurements, Cresyl violet was used to stain all cortical layers. Measurements were done using ImageJ. Layer 1 width was measured from 3 sections and both hemispheres and averaged for each mouse and graphed. All measurements were then analyzed using an unpaired Student's T-test.

For cell number counts, a rectangular macro was created in ImageJ and aligned over the primary somatosensory cortex over cortical Layers 2-5 and aligned over the apex of the hippocampus. The hippocampus was used to ensure similar comparable sections were selected. 3 sections were analyzed and averaged for each animal.

qRT-PCR analysis

P16-P18 mouse neocortex was homogenized in Trizol. RNA was extracted with chloroform and purified with RNEasy Mini kit (Qiagen). RNA yield and quality were quantified by nanodrop and reverse transcribed into cDNA was made with iScript™ Reverse Transcription Supermix (Bio-Rad). qPCR was performed using iTaq™ Universal SYBR® Green Supermix green (Bio-Rad), and Step One Plus (Applied Biosystems). Each reaction was performed in triplicate, using 30-100 ng cDNA per reaction and normalized to endogenous control β-actin. The KiCqStart SYBR® Green primers (Sigma Aldrich) used are detailed in Table 3. Fold change in expression relative to the control group was determined using the ΔΔCt algorithm method. ΔCt was normalized to the housekeeping gene, β-actin.

Seizure observation

Mice were observed and handled between P7 to P12 for 5 minutes, two mornings a week. Additionally, we observed the untreated mice for 1 hour following handling between the ages of P16-18. Of note, several mice died after 1 seizure, while others had multiple observed seizures and died unobserved.

Seizure observation during rapamycin treatments

Each morning of treatment, starting at P7, the cage was first observed prior to taking the lid off for any mouse seizures. Then each mouse that was to be treated was treated with IP injection of rapamycin or vehicle and then observed between 5-15 minutes following treatment 3 days a week (M, W, F mornings). During the 5-15 minutes following treatment mice were handled 2-3 more times for a duration of 30 seconds.

EEG

Video/EEG recording was performed on mice at P16-18 with a modified protocol from what has been conducted previously by the Neuromodels Core Facility at UTSW Medical Center (Cho et al., 2015). The day of EEG recording, mice were stereotaxically implanted with recording electrodes under isoflurane anesthesia. Four epidural electrodes made from #00-90 × 1/8 inch stainless steel screws were placed over the left parietal cortex, right parietal cortex, olfactory bulb, and cerebellum. The reference electrode was placed over the olfactory bulb and cerebellum was utilized as ground. Electrodes were attached by a flexible wire (Kynar, 30 gauge) to a custom 6-pin micro connector (Omnetics) and secured with dental acrylic. Mice were monitored post implantation and given 4 hours to recover. Mice were then placed in a custom acrylic recording cage (Marsh Designs) and connected to a Tucker-Davis Technologies RZ2/PZ3 neurophysiology

workstation through a flexible cable suspended from the top of the cage with an interposed commutator to allow mice free access to food and water without twisting the cable. Continuous video/EEG (300 Hz sampling) was recorded for each mouse simultaneously for 12 hours and data was converted to Matlab format where spectral analysis was conducted by a user blinded to the experimental grouping for the presence of seizures and epileptiform activity. Waveform traces were visualized with LabChart 8 Reader and correlated with time-stamped behavioral changes. An event qualified as a seizure if it had a 4 Hz or greater frequency, lasted 5 or more seconds, and had an amplitude 100% greater than baseline (Cho et al., 2015).

Histology

Mice were perfused from P16-P18 and the extracted brains were fixed in 4% paraformaldehyde overnight. Brains were switched to 30% sucrose in PBS the following day. 3 days later, brain was frozen in a mold filled with 1:1 ratio OCT to 30% sucrose in PBS solution. 25μm coronal slices were cut using a cryostat and mounted onto Superfrost slides. Cresyl violet standard staining protocol was followed. Slides were imaged on the NanoZoomer in the UT Southwestern Whole Brain Microscopy Facility, and analyzed on NanoZoomer Digital Pathology software.

Rapamycin treatments

Rapamycin was dissolved in 0.25% polyethylene glycol and 0.25% tween. Litters of pups were treated with either 6 mg/kg rapamycin or vehicle administered by IP injection starting at P7. Mice were treated and weighed every Monday, Wednesday, and Friday(Tsai et al., 2012). Treatment continued until 6 weeks of age. During treatments, mice were observed for seizures for 10-20 minutes post injection.

Probenecid treatments

Probenecid was dissolved in 1N NaOH and 10% PBS, then titrated up to pH 6.2-7.6 with 1N HCl to create a white suspension and diluted with 25% w/v propylene glycol. Mutant mice were treated with either 100mg/kg Probenecid or 25% w/v propylene glycol by IP injection starting at P12. Treatment was given daily, TID. During treatments, mice were observed for seizures for 10-20 minutes post injection. All observed seizures were included in our seizure quantification.

Proteomics

Protein was extracted from neocortical tissue from P15-16 male and female mice in RIPA buffer 1% NP40 and 1% SDS. Amount of protein was quantified with Pierce™ BCA Protein Assay Kit (ThermoScientific). 50μg of protein was loaded into each well of a TGX gel (Bio-Rad), run on the gel and processed for Liquid Chromatography/ Mass Spectrometry (LC-MS) run by the UT Southwestern Proteomics Core.

Gel band samples were digested overnight with trypsin (Promega) following reduction and alkylation with DTT and iodoacetamide (Sigma–Aldrich). The samples then underwent solid-phase extraction cleanup with an Oasis HLB plate (Waters) and the resulting samples were injected onto an Orbitrap Fusion Lumos mass spectrometer coupled to an Ultimate 3000 RSLC-Nano liquid chromatography system. Samples were injected onto a 75 μm i.d., 75-cm long EasySpray column (Thermo) and eluted with a gradient from 0-28% buffer B over 180 min. Buffer A contained 2% (v/v) ACN and 0.1% formic acid in water, and buffer B contained 80% (v/v) ACN, 10% (v/v) trifluoroethanol, and 0.1% formic acid in water. The mass spectrometer operated in positive ion mode with a source voltage of 1.9-2.2 kV and an ion transfer tube temperature of 275°C. MS scans were acquired at 120,000 resolution in the Orbitrap and up to 10 MS/MS spectra were obtained in the ion trap for each full spectrum acquired using higher-energy collisional dissociation (HCD) for ions with charges 2-7. Dynamic exclusion was set for 25 s after an ion was selected for fragmentation.

Raw MS data files were analyzed using Proteome Discoverer v2.2 (Thermo), with peptide identification performed using Sequest HT searching against the mouse protein database from UniProt. Fragment and precursor tolerances of 10 ppm and 0.6 Da were specified, and three missed cleavages were allowed. Carbamidomethylation of Cys was set as a fixed modification, with oxidation of Met set as a variable modification. The false-discovery rate (FDR) cutoff was 1% for all peptides and proteins, and only proteins with at least 2 peptide spectral matches were considered.

We submitted two batches of samples, 3 controls and 3 mutants were in each batch. (6 controls and 6 mutants total). Analysis was performed and figures created through the Perseus platform(Tyanova et al., 2016). The data was normalized with a log transformation and quantized with Z-score, and cluster normalization. Heatmap displays significance results from Benjamini-Hochberg FDR 0.01 cutoff. Functional enrichment analysis includes significant results with cutoff of permutation-based FDR 0.05. Functional enrichment was analyzed with FunRich Software(Pathan et al., 2015). Epilepsy-related proteins were sorted by categories outlined in a recent review article with genes that have a 1) strong causal epilepsy only phenotype, 2) neurodevelopmental disorder with epilepsy, 3) systemic disease with epilepsy, and those that are 4) epilepsy related, but the link to epilepsy requires more in-depth research(Wang et al., 2017).

Metabolomics

Metabolites were extracted from neocortical and cerebellar tissue from P15-16 mice. To optimize extraction for neurotransmitters the tissue was homogenized in acetonitrile and formic acid following a previously reported protocol(Wojnicz et al., 2016). Heavy internal standards were spiked in during the preparation of the lysate. LC-MS/MS was performed in collaboration with the UT Southwestern Metabolomics Core.

LC-MS/MS system

Mass spectrometric analyses were performed on Sciex "QTRAP 6500+" mass spectrometer equipped with an ESI ion spray source. The ESI source was used in both positive and negative ion modes. The ion spray needle voltages used for MRM positive and negative polarity modes were set at 5000 V and −4500 V, respectively. The mass spectrometer was coupled to Shimadzu HPLC (Nexera X2 LC-30AD). The Analyst 1.6.3 software controls the whole LC-MS/MS system.

Chromatography

Chromatography was performed under reverse phase conditions using an ACE 3 C18-PFP column 4.6 mm × 150 mm (Advanced Chromatography Technologies Ltd, Scotland). The column temperature, sample injection volume, and the flow rate were set to 30°C, 5 μL, and 0.5 mL/min respectively. The HPLC conditions were as follows: Solution A: 0.2% formic acid in water (LC-MS grade) and Solution B: Acetonitrile (LC-MS grade). The chromatogram was run under gradient condition as follows: 0-2 min at 95% (A) and 5% (B), 2-5min increasing eluent B to 90%, 5-16 min at 90% (B), 17-25min: 95% (A) and 5% (B)

SCIEX MultiQuant 3.0.3 software was used for data processing. Relative quantification was performed based on the peak area of each metabolite.

Analysis

Samples were normalized to a heavy amino acid internal standard and then to total ion chromatogram (TIC). The data was normalized with a log transformation and normalized with Z-score. Student t-test permutation-based FDR q values were used to test for significance. Perseus was utilized to normalize and analyze the data. Peaks were confirmed with pure samples for neurotransmitters and significantly affected amino acids.

Acute slice recordings

Acute slice recordings were performed as detailed below (Tsai et al., 2012).

Acute brain slice preparation

Acute coronal brain slices were prepared from pups, P16-20, that were anesthetized with isoflurane (Forane®, AbbVie) and decapitated. Brains were rapidly removed and immersed in ice-cold oxygenated protective artificial cerebrospinal fluid (aCSF,95% O2, 5% CO2) containing (in mM): 125 NaCl, 26 NaHCO3, 1.25 NaH2PO4, 2.5 KCl, 1 MgCl2, 2 CaCl2, and 25 glucose (equilibrated with 95% O2 and 5% CO2., osmolarity: ~310 mOsm/kg, Ph adjusted to 7.4 with NaOH). The brains were trimmed with a scalpel blade and glued onto the stage of a vibrating microtome (VT1200S, Leica Microsystems). Coronal slices (thickness 300 μm) containing somatosensory cortex were cut in oxygenated ice-cold protective aCSF and subsequently incubated at 32°C for 25 minutes. After this recovery period, the slices were kept at room temperature for at least 30 minutes before the electrophysiological recordings.

Electrophysiological recordings and stimulation

Sections were visualized in a recording chamber and continuously perfused with oxygenated standard aCSF (2–3 mL/min). Visually guided (infrared DIC video microscopy and water-immersion 40x objective) whole-cell recordings were obtained with patch pipettes (4–6 MΩ) pulled from borosilicate capillary glass (World Precision Instruments) with a Sutter P-1000 horizontal puller. Electro-physiological recordings were performed in the recording chamber at 31–33°C. Cortical neurons on the slice were visualized by microscopy with IR light source with DIC imaging and filled cells with Neurobiotin following recording to post hoc visualize each cell with fluorescent microscopy and confocal microscopy. The internal solution contained (in mM): 150 K-gluconate, 3 KCl, 10 HEPES, 0.5 EGTA, 3 MgATP, 0.5 GTP, 5 phosphocreatine-tris2, and 5 phosphocreatine-Na2. pH was adjusted to 7.2 with NaOH. Experiments were conducted with Axon Instruments hardware and software (Multiclamp 700B, Digidata 1550A, and pClamp 10). Recordings were sampled at 10 kHz using a MultiClamp 700B and Digidata 1550A system (Molecular Devices).

Miniature EPSCs and evoked EPSCs were recorded at −70 mV in ACSF containing 1 μM tetrodotoxin (TTX) and/or Picrotoxin (20 μM), whereas miniature IPSCs and evoked IPSCs were recorded at +10 mV in the presence of 1 μM TTX, and 5 μM (RS)-CPP 5 μM and 2,3-dioxo-6-nitro-1,2,3,4-tetrahydrobenzo[f]quinoxaline-7-sulfonamide (NBQX). In order to measure the effects of glycine, we recorded mEPSCs with and without strychnine (1 μm) or with and without 7-Cl-KYNA (20μM). mIPSCs were recorded with and without strychnine (1 μm), picrotoxin (20μm), were individually recorded. Visually guided (infrared DIC video microscopy and water-immersion 40x objective) whole-cell recordings were obtained with patch pipettes (4-7 MΩ) pulled from borosilicate capillary glass (World Precision Instruments) with a Sutter P-1000 horizontal puller. Recordings were included only when a GΩ seal formed prior to whole-cell access. Recordings were analyzed offline using Clampfit 10-6. A first-pass automated detection of putative miniature synaptic events was conducted based on an amplitude threshold of 5 pA. Each putative event was then manually scrutinized and visually confirmed or rejected as a synaptic event. The threshold stimulus amplitude was defined as 5 times greater than the median absolute deviation of the 10-millisecond baseline preceding the stimulus. Access resistance was frequently checked to be <30 MΩ and stable (less than 20% variability).

The internal pipette solution contained (in mM): 140 Cs-methanesulfonate, 15 HEPES, 0.5 EGTA, 2 TEA-Cl, 2 MgATP, 0.3 NaGTP, 10 phosphocreatine-tris2, 2 QX 314-Cl. pH was adjusted to 7.2 with CsOH. A concentric bipolar stimulating electrode was kept at 100 microns longitudinally below. Every attempt was made to only have the tip of the stimulating electrode within the tissue and in Layer 2/3 to stimulate the target pyramidal neuron within the barrel column of the barrel cortex in somatosensory region.

Evoked EPSCs and Evoked IPSCs were measured at multiple strengths above threshold stimulation level. PPR of eEPSC was measured with 20Hz 50ms stimulation and eIPSC with 10Hz 100ms stimulation.

Whole-cell patch clamp recordings were obtained from pyramidal cells in Layers 2/3 of the somatosensory cortex. Pyramidal neurons were distinguished from interneurons by their shape, spiking pattern and action potential waveform shapes. In addition, their identity was confirmed by their large apical dendrites, which were visualized by using NEUROBIOTIN® Tracer (Vector, SP-1120) in combination with Alexa 488-streptavidin staining.

QUANTIFICATION AND STATISTICAL ANALYSIS

Statistical parameters can be found in figure legends. All datasets were tested for normality to determine appropriate statistical tests. Significance was defined as having a p-value<0.05. For proteomics and metabolomics data, significance was defined as having a permutation-based q-value<0.05.

Sample sizes are described in figure legends of the manuscript. We chose the sample sizes based on previous literature, common standards in the field, our own experience, and experimental feasibility. An appropriate number of technical and biological replicates were generated under similar conditions yielding statistically significant results between groups. Results with no significant difference after being tested multiple times were deemed non-significant.

Experiments were performed multiple times (mostly in triplicates) with biological replicates unless otherwise noted in the methods or figure legends. For immunohistochemistry three slices per mouse were

analyzed, and three biological replicates per condition. Two to three biological replicates were used for western blot analyses.

No randomization was applied in this study because experiments required separation by genotype and drug treatments. Mice were selected based on age and genotype. Males and females were used and distributed in controls and mutants.

Investigations were performed blinded to studies. However, for *in vivo* studies, blinding was impacted by mutant mice having a distinct small size and rounded head shape.